Modeling and Upscaling of Deformation Bands in Fault Damage Zones

Master of Science Thesis in Applied Mathematics

Livar Lima

Department of Mathematics
University of Bergen

May 18, 2008

Preface

All good things come to an end, also my time as a student at the university. First, I would like to thank my supervisor, professor Magne S. Espedal, for always being enthusiastic, positive and willing to help. Sylvie Schuller deserves thanks for constructive feedback when it comes to geology and Dmitriy Kolyukhin must be mentioned for letting me use his code and for interesting discussions. To all the others who have contributed in my thesis, thank you!

I would also express my gratitude to the present and former students at the Department of Mathematics for a good and friendly atmosphere. Among them, I would like to emphasize Jørn Hafver for many inspiring conversations and unforgettable memories throughout the years as students at the university.

Finally, I would like to thank my family. Especially, my mother and father for always believing in me and for all great support you have given me. I am grateful for having such fabulous parents!

Livar Lima
Bergen, May 2008

Contents

Chapter 1

Introduction

When we want to model flow in a reservoir, a reservoir simulator is needed. Typical reservoir simulators can handle on the order of $10^5 - 10^6$ simulation cells, but the exact number will vary depending on the type of simulation to be performed and the computer hardware. Geological characterizations typically contain on the order of $10^7 - 10^9$ cells. We often refer to these models as fine scale models. We want to transfer the most important information from the fine scale to a coarser scale in order to speed up the use of the reservoir simulator or, more dramatically, be able to use the simulator for practical purposes.

When we are trying to model or describe physical processes and properties of a reservoir, it is important to know that the data we are using may come from different scales. The data which we use in order to form a geological model, are collected at many different scales in the reservoir, i.e. log-, seismic- and core-plug-data, see Figure 1.1.

Hence, there are a lot of upscaling processes on the way from the millimetre-level to the seismic-data on a 10-meters-level. This process can result in a geolocical model containing millions of cells. The molecular scale is the smallest scale on which we are able to describe properties of single molecules and their interactions. If we were using this scale to construct a flow model we would deal with a very large number of molecules. From a practical point of view, it is not advantageous to do computations on this scale. If we assume that the matter is continuous, we obtain the pore scale. At this scale, different phases can be shown. We can also observe interfaces between the fluids themselves and between a fluid and the rock. Navier-Stokes equations describe those phenomena on the pore scale well. If we average the pore scale over a representive elementary volume (REV) with size V, the local scale is obtained. REV must be chosen such that it is larger than the microscopic length V_m, but smaller than the large scale variations V_M such that the mi-

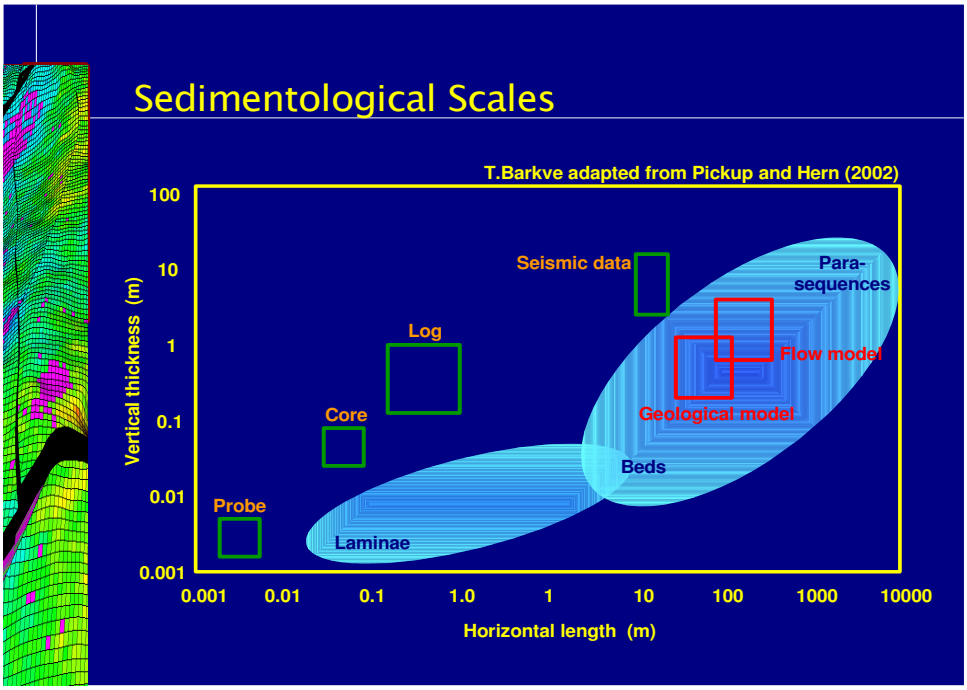

Figure 1.1: Differences in scales. From a presentation by T. Barkve, 2005.

croscale variations are smoothed out and the large scale heterogeneities are obtained, see Figure 1.2. At the local scale, continuum model parameters such as porosity and saturation occurs.

Flow models are based on data from geological models, see Figure 1.1. The upscaling procedure from the geological model to the flow model is less dramatic than all the upscaling processes which must be done in order to form a geological model.

In upscaling methods, in the following defined as the upscaling procedure from a geological model to a flow model, the challenge is to construct a coarse scale so that the most important information from the geological fine scale such as velocity, saturation and pressure are taking into account. Unfortunately, there doesn't exist any general way to do this upscaling procedure. It depends highly on the geology and what parameters we want to upscale.

It is common to classify different upscaling procedures in terms of what type of parameter that are upscaled. In a single-phase flow, absolute permeability and the porosity are the only parameters to be upscaled. Such an approach is called "single-phase upscaling" and the pressure equation is modified. For a two-phase flow, the parameters we can upscale are porosity, absolute permeability and relative permeability. If we have a two-phase flow,

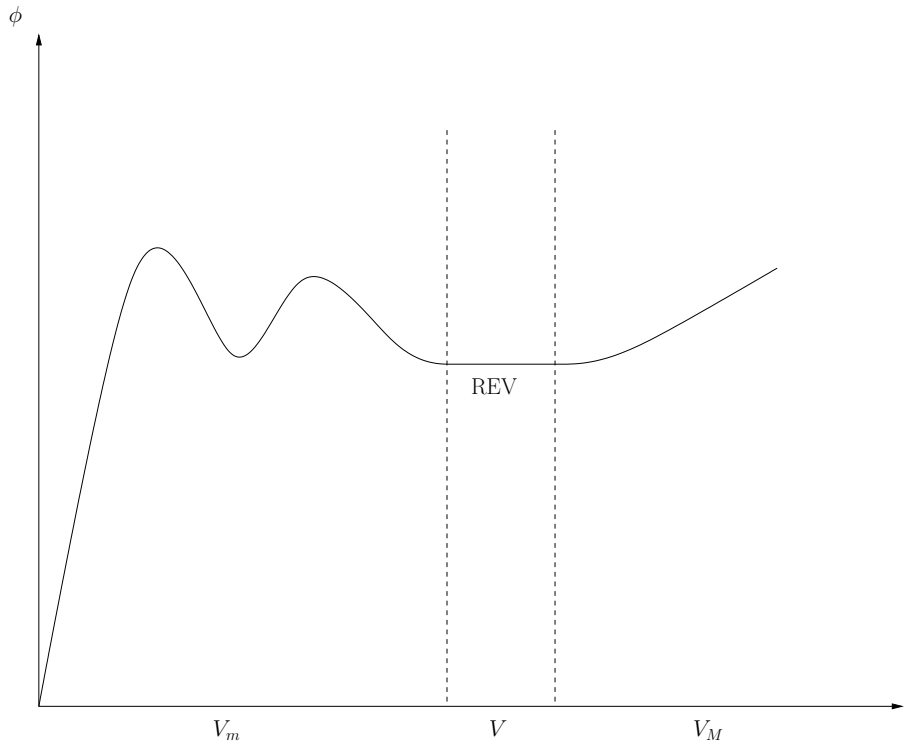

Figure 1.2: An average of the pore scale is taken over a representive elementary volume (REV) with size V in order to obtain the local scale.

we call the procedure "two-phase upscaling". In two phase upscaling procedures, we need to modify both the pressure equation and the saturation equation. These equations are defined in Chapter 2. We will in this thesis not discuss multiphase fluid flow, but Christie (10) presents a review on developments in methods for scale-up of multi-phase flow in porous media.

In addition to classify the upscaling procedure as single-, two or multiphase flow, we have another type of classification - local and global calculations. For a local method, the only information which is of interest is the gridblocks included in the area we want to upscale. In other words, we compute coarse scale parameters by only consider a fine scale region corresponding to a target coarse block. If we are using a global model, the information is given on a larger area and we need more gridblocks. In order to calculate the coarse scale parameters, we must in most global upscaling approaches run a simulation on the entire fine scale model.

It is possible to combine a local and a global method. An example would be if we were solving a single-phase problem globally. The solution now gives

us boundary conditions for a fine problem which we can upscale. Then we solve a coarser problem with the information from the fine problem. We continue in this manner until we get an acceptable result.

Many questions arrise when we want to perform an upscaling procedure. Do the partial differential equations that model porous media flow at the coarse scale level represent the porous media flow at the fine scale level with acceptable results? How should we represent the heterougeneties at the fine scale level on the coarse scale level? Today, no one has answered these questions good enough. A lot of the existing upscaling techniques are based on local average procedures, but they are not sensitive to a perturbation in the global large scale conditions for the elliptic pressure equation.

We know that boundary conditions have a great influence on the flow patteren in the porous media and that we will get different flow patterns according to the upscaling technique we use. Boundary conditions are therefore important to discuss in order to get reliable coarse scale model for porous media flow. In Section 3.1.5, we discuss two choises of boundary conditions for a local upscaling procedure - fixed boundary conditions and periodic boundary conditions. The fluid flow will also depend on the size and structure of the grid. Wu et al. (42) discuss upscaling permeability errors due to the connection between the imposed boundary conditions and the grid size when the underlying medium is periodic at small scales. Unfortunately, analysing the upscaling process of general heterogenous media is much more difficult since a different pressure solution leads to different values for the permeability. It must be mentioned that there exists upscaling techniques which give rigously answer to the questions arrised above, but they are all based on ideal heterogenous formations and therefore not interesting for practical purposes.

There are indeed several reviews on upscaling techniques, i.e. Durlofsky (17) and Farmer (21).

Chapter 2 gives a overview of reservoir mechanics and the basics of reservoir modeling are introduced. Flow-based upscaling procedures are presented in Chapter 3. In Chapter 4 we describe typically geological properties of faulted and fractured porous media that will influence the numerical simulations. Then in Chapter 5 we will describe the workflow for creating the numerical model. Further in Chapter 6 we are focusing on upscaling of deformation bands and results are also given in this chapter. In Chapter 7 two upscaling algorithms for a fault damage zone are presented. We finish the thesis with a summary and some conclusions in Chapter 8. Topics for further work is also pointed out in this chapter.

Chapter 2

The Mathematical Model

For a rock to act as a reservoir, it must have pores containing a fluid and the pores must be connected such that the fluids are allowed to flow within the reservoir. A phase can be a composition of several components and these components can sometimes be different fluids. In reservoir modeling we are usually focusing on three fluids - oil, gas, and water. We refer to them as three phases, but if the pressure is low enough, some oil will evaporate into gas. Then we say that we have a composition of gas in the oil phase. In this chapter we will give some useful definitions for a reservoir and state the equations which describe flow in porous media. More general information about reservoir mechanics can be found in references (11), (34), (35) and (41).

2.1 Pore Scale Dynamics

On the pore scale level, the capillary pressures are the dominating forces. In this section we will discuss the dynamics on a pore scale.

2.1.1 Wettability

When different fluids are flowing in a pore, we will observe surface tension between the fluids itself and between the fluids and the surface of the pore. These forces are important to understand when we want to describe flow in porous media. In Figure 2.1, we can see that the water spreads out on the surface of the media. In this case, the media is wetting. We have another situation in Figure 2.2. Here the media is non-wetting. In order to classify whether a media is wetting or non-wetting, we must examine the angle θ. If $\theta > \frac{\Pi}{2}$ the media is wetting. If $\theta < \frac{\Pi}{2}$, the media is non-wetting.

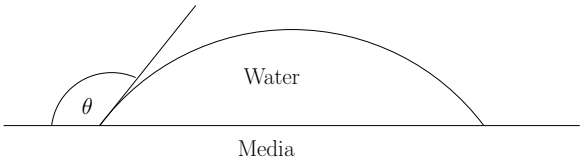

Figure 2.1: The media is wetting.

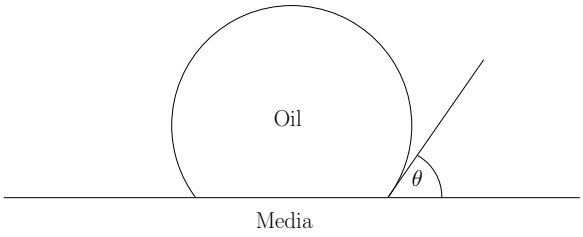

Figure 2.2: The media is non-wetting.

It is common to give parameters such as capillary pressures as a function of the wetting fluid.

2.1.2 Saturation and Capillary Pressure

If there are two or more fluids in a reservoir, we need a measure for the fraction of one fluid, relative to the total amount of fluid in the pore system. We therefore define the amount of fluid j as follows

$$S_j = \frac{\text{the volume of fluid } j}{\text{the volume of all connected pores}} \quad .$$

The saturation is a dimensionless parameter and we assume that the connected pores are fully filled with a fluid. Thus we have that

$$\sum_{j}^{n} S_j = 1 \quad . \tag{2.1}$$

Capillary pressure plays an important role when a fluid invade a reservoir which already contains a fluid. There will be interfacial tensions between the different fluids and the matrix of the reservoir. As a consequence, the pressure in the wetting phase will be smaller than the pressure in the non-wetting phase. We call the difference due to the interfacial tension for capillary pressure. The capillary pressure depends on the size of the pores in the

reservoir and on the relation between the wetting and non-wetting phase. For a small value of P_c, only pores with large radius will be filled with a non-wetting fluid. By increasing P_c, smaller and smaller pores will be filled.

The entery pressure is given as a function of the wetting phase saturation and it is called the Young-Laplace equation. It is given as follows

$$P_c(S_w) = p_{nw} - p_w = \frac{2\sigma}{r} \cos\ \theta \quad , \tag{2.2}$$

where p_{nw} and p_w is the pressure of the non-wetting and wetting fluid, respectively, σ is the surface tension, r is the radius in the pore and θ is the angel between the fluids. The Young-Laplace equation tells us how fluids are distributed within the pores. In Sorbie and van Dijke (36) they give a lot of examples of how the capillary pressure controls the distribution of the fluids in the pores.

2.2 Continuum Model Parameters

A reservoir is a porous medium which consists of pores and a matrix. In the matrix which is a solid rock, no flow is possible when we restrict ourselves to the local scale. We call the volume of all pores and the matrix a block volume. Since we are building a mathematical model in order to describe the flow of fluids, we are only interested in the connected pores where the fluids can flow. Therefore it is appropriate to define an effective porosity as follows

$$\phi \equiv \frac{V_p}{V_b} \quad , \tag{2.3}$$

where V_p represents the volum of the connected pores and V_b the block volume of the porous media.

At the continuum scale, the effect of the capillary pressure is reduced and the dominating parameters are the viscosity and the gravity force.

2.2.1 Permeability

The permeability depends on the rock and it tells us how easy a fluid will flow through the pores of the porous medium. When studying single-phase flow, we only have an absolute permeabilty. We can represent the permeability as a scalar if the media is homogenuos and isotropic. In a homogenous reservoir, the value for the permeabilty is constant. For the opposite case, a heterogenous medium, it can vary with the position in the media. If the permeability is the same in all directions, the media is isotropic. Otherwise,

we say that the media is anisotropic. In general, the permeabilty is a tensor. If the permeabilty tensor is symmetric and positive definite, we know by the Onsager's principle that we have a physical consitent conductivity. We can always transform a symmetric and positive definite tensor into a diagonal form, but such a transformation results in loss of information.

2.2.2 Relative Permeability

When two or more fluids are flowing in a reservoir, relative permeability will be involved if we want to describe the motion of fluids. Since only one fluid can flow through a pore at a given time, there will be some additional effects between the fluids. This effect is called relative permeability and it depends on the saturation.

2.2.3 Viscosity

Viscosity is a property for fluids. It is common to assume that the viscosity is constant, but for gases the viscosity will vary with the pressure. In this thesis, we assume that the viscosity is constant.

2.2.4 The Mass Conservation Law

Conservation laws describe how a physical quantity is conserved whithin a closed system. We will derive the conservation law for mass, which is commonly used in reservoir modelling.

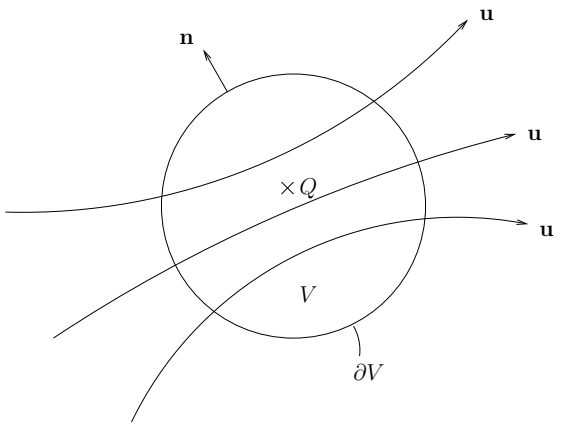

Figure 2.3: An arbitary closed volume V with a flux passing through the volume.

Assume we have an arbitrary geometric volume V, see Figure 2.3. The conserved mass in a porous media is given by $\Gamma = \rho\phi$. We let a quantity q of Γ flow through the surface of the volume V per timeunit. Hence q is the flux of Γ, and we will have that $q = \rho\mathbf{u}$. Let $\mathbf{n}$ be a outward normalvector to ∂V and let Q be the term for any prospective source or sink in V. For the mass to be conserved within the volume V, we must have

$$\int_V \frac{\partial(\rho\phi)}{\partial t} dV + \int_{\partial V} (\rho\mathbf{u}) \cdot \mathbf{n} ds = \int_V Q dV \quad . \tag{2.4}$$

By using the divergence theorem, see for example Apostol (3, p. 457-460), we obtain the conservation law for mass on an integral form

$$\int_V \left[\frac{\partial(\rho\phi)}{\partial t} dV + \nabla \cdot (\rho\mathbf{u}) \right] dV = \int_V Q dV \quad . \tag{2.5}$$

Since we have assumed that the volume V is arbitary, we can state the differential form

$$\frac{\partial(\rho\phi)}{\partial t} + \nabla \cdot (\rho\mathbf{u}) = Q \quad . \tag{2.6}$$

2.3 Fine Scale Equations

We will here present the equations describing single and two-phase flow on the fine scale. As in many other reservoir problems, Darcy's law combined with the statement of mass conservation is essential.

2.3.1 Darcy's Law

We will describe the motion of phases in a porous media by using Darcy's law. Orginally, Darcy's law was a result after a lot of experiments where different fluids have flown through different porous medium, see reference Darcy (12), and was thus considered as an emperical law. It is possible to derive Darcy's law by a volume averaging of the Navier-Stokes momentum equations. The modern form of the Darcy's law on a differential form can be stated as follows

$$\mathbf{u} = -\frac{K}{\mu}(\nabla p + \rho g \mathbf{k}) \quad , \tag{2.7}$$

where K is the permeability tensor, μ is the viscosity, p is the pressure, ρ is the density and g is the acceleration of gravity.

The Darcy-velocity is a macroscopic velocity, and hence it is the virtual velocity of the fluid we are describing. Another important point to be aware of is that the Darcy's law can only be used for slow velocities and when the friction between the moving fluid and the matix have an effect on the flow. In a reservoir model, these two assumptions are in most cases fulfilled.

2.3.2 Single-phase Flow Equations

Despite from Darcy's law, Equation (2.7) and the mass conservation law, Equation (2.6), the pressure equation is essential for single phase flow. It is obtained by combining Darcy's law without gravity and the mass conservation law. The pressure equation is then given by

$$\frac{\partial}{\partial t}(\phi\rho) - \nabla \cdot (\frac{\rho}{\mu} K \cdot \nabla p) + Q = 0 \quad . \tag{2.8}$$

where all magnitudes have been defined earlier.

2.3.3 Two-phase Flow Equations

As in the case of the one-phase flow equation, the pressure equation can again be formed by combining Darcy's law with a statement of mass conservation. Since this is a two-phase flow situation, the permeability tensor is multiplied with the relative permeability of phase j. Darcy's law becomes

$$\mathbf{u}_j = -\frac{k_{rj}}{\mu_j} K \cdot \nabla p_j \quad , \tag{2.9}$$

where the subscribt j refers to the phase ($j = w$ for water and $j = o$ for oil) and k_{rj} is the relative permeability for phase j.

For two-phase flow equations, the mass conservation is given by

$$\frac{\partial}{\partial t}(\phi\rho_j S_j) + \nabla \cdot (\rho_j \mathbf{u}_j) + Q_j = 0 \quad , \tag{2.10}$$

where all magnitudes have been defined earlier.

We can also state the pressure equation for the two-phase flow by putting Equation (2.9) into Equation (2.10). First, we define the mobility as

$$\lambda_j(S) = \frac{k_{rj}(S)}{\mu_j} \quad , \tag{2.11}$$

where j referes to the fluid, i.e. water (w) or oil (o). Models with high mobility ratio, i.e. a water-air model, will give a stronger coupling between the pressure/velocity and the saturation equation we soon will present. By using

the definition of mobility and assuming that the fluids are incompressible, we obtain the pressure equation for two-phase flow

$$\nabla \cdot (K\lambda(S) \cdot \nabla p) = Q \quad , \tag{2.12}$$

where $\lambda(S) = \lambda_w(S) + \lambda_{nw}(S)$ is usually a U-shaped function of saturation. The index w is the wetting phase and the index nw is the non-wetting phase. All the other magnitudes have been defined earlier.

When it comes to the saturation equation for two-phase flow, we assume that the flow is immiscible and incompressible. We also neglect the gravity forces and we will describe the displacement of oil by water. The saturation equation is formulated as follows

$$\phi \frac{\partial S}{\partial t} + \nabla \cdot (f(S)\mathbf{u}) - \epsilon \nabla \cdot (D(S,x) \cdot \nabla S) = Q \quad , \tag{2.13}$$

where S is the saturation of the wetting phase, $\mathbf{u}$ the Darcy velocity and $f(S)$ is the convensional flow function defined by

$$f(S) \equiv \frac{\lambda_w(S)}{\lambda_w(S) + \lambda_{nw}(S)} \quad . \tag{2.14}$$

The convensional flow function is typically a S-shaped function and will for that reason establish a shock in the saturation equation after some time. We also have a bell shaped diffusion function, given by

$$D(S,x) = -K(x)f(S)\lambda_{nw}(S)\frac{\partial P_c}{\partial S} \quad , \tag{2.15}$$

where $P_c(S,x)$ is the capillary pressure.

The diffusion function in the saturation equation, Equation (2.13), is scaled by a dimensionless parameter ϵ. When ϵ is small, we can see from this equation that the information about the heterogenitiy in the media comes from the pressure-velocity equations through $\mathbf{u}$ since $K(x)$ is represented by $D_{pc}(S,x)$.

2.4 The Buckley-Leverett Equation

The Buckley-Leverett equation is a transport equation which describe two-phase flow in porous media. In order to derive this equation, we consider the following assumptions:

1. Two-phase, immiscible fluid flow in one dimension.

2. Neglect capillary pressure.

3. Incompressible fluids.

4. The viscosity is constant and the porous media is homogenous.

5. The porous media is filled with as much fluid as possible which means that $S_w + S_{nw} = 1$.

We use the conservation law for two-phase flow, Equation (2.10), with no source or sink term. By using the assumptions listed above, we get

$$\frac{\partial u_w}{\partial x} + \phi \frac{\partial S_w}{\partial t} = 0 \quad , \tag{2.16}$$

$$\frac{\partial u_{nw}}{\partial x} + \phi \frac{\partial S_{nw}}{\partial t} = 0. \tag{2.17}$$

Now we add these two equations

$$\frac{\partial}{\partial x}(u_w + u_{nw}) + \phi \frac{\partial}{\partial t}(S_w + S_{nw}) = 0 \quad . \tag{2.18}$$

By assumption number 5 we get

$$\frac{\partial}{\partial x}(u_w + u_{nw}) = 0 \quad . \tag{2.19}$$

Hence $u_w + u_{nw} = C = u$, which is similar to assumption number 3. Since we have neglected the capillary pressure and the fact that we only have one dimensional flow, Darcy's law for the wetting and non-wetting fluid becomes

$$u_w = -K\lambda_w(\frac{\partial p}{\partial x} + \rho_w g \cos\theta) \quad , \tag{2.20}$$

$$u_{nw} = -K\lambda_{nw}(\frac{\partial p}{\partial x} + \rho_{nw} g \cos\theta) \quad . \tag{2.21}$$

By solving these two equations for $\frac{\partial p}{\partial x}$, we get

$$\frac{u_w}{K\lambda_w} + \rho_w g \cos\theta = \frac{u_{nw}}{K\lambda_{nw}} + \rho_{nw} g \cos\theta \quad . \tag{2.22}$$

We replace the velocity of the non-wetting phase by putting $u_{nw} = u - u_w$ and by re-ordering Equation (2.22), we achieve the following expression

$$u_w(\frac{1}{\lambda_w} + \frac{1}{\lambda_{nw}}) = \frac{u}{\lambda_{nw}} + K(\rho_{nw} g - \rho_w g)\cos\theta \quad . \tag{2.23}$$

We define a gravity parameter Γ by

$$\Gamma \equiv (\rho_{nw} g - \rho_w g) \cos\theta \quad , \tag{2.24}$$

and we can now write all quantities which depend on the wetting-saturation on the right side of the following equation

$$\frac{u_w}{u} = \frac{\lambda_w}{\lambda_w + \lambda_{nw}} + \frac{\lambda_w \lambda_{nw}}{\lambda_w + \lambda_{nw}} \frac{K}{u} \Gamma \quad . \tag{2.25}$$

As we mentioned in Section 2.1.2, it is common to give saturation as a function of the wetting fluid. From now on, we skip the wetting index on the saturation-quantity which means that the saturation-quantity without index refers to the wetting fluid. The fractional flow is defined by

$$F(S) \equiv \frac{u_w}{u} \quad . \tag{2.26}$$

The fractional flow function contains two parts as we can see from Equation (2.25). The convectional flow $f(S)$, given in Equation (2.14), and the gravity term defined by

$$f_g(S) \equiv \lambda_{nw}(S) f(S) \frac{K}{u} \Gamma \quad . \tag{2.27}$$

Hence, we can write the fractional flow equation as $F(S) = f(S) + f_g(S)$. Putting in $u_w = F(S)u$ in Equation (2.16), we can finally state the Buckley-Leverett equation

$$\frac{\partial S}{\partial t} + \frac{u}{\phi} \frac{\partial F(S)}{\partial x} = 0 \quad . \tag{2.28}$$

Chapter 3

Flow-based Upscaling Procedures

From the set of parameters in the reservoir flow equations, we know that the permeability has the greatest influence on the flow in the porous media. This is a conclusion from Tjølsen and Damsleth (38). We are focusing on upscaling of permeability in this thesis. Since flow based upscaling algorithms are considered to perform best for permeablility, we will restict this chapter to flow based upscaling techniques. In such cases the upscaling problem is to find, for each K, a corresponding K^* such that the solution of the coarse problem is close to the solution of the fine scale problem. Taking into account multiphase flow problems, we add significantly complexity to this picture. We will use definitions and equations stated in Chapter 2.

3.1 Single-Phase Upscaling

We can see from Section 2.3 in Chapter 2 that single-phase flow without gravity and source terms, is described by Darcy's law,

$$\mathbf{u} = -\frac{1}{\mu} K \cdot \nabla p \quad , \tag{3.1}$$

and the mass conservation equation,

$$\nabla \cdot \mathbf{u} = 0 \quad , \tag{3.2}$$

where we have assumed that the phase and rock are incompressible (i.e. the porosity ϕ and the density ρ does not vary in space or time). By combining these two expressions, we obtain the elliptic pressure equation

$$\nabla \cdot (\frac{K}{\mu} \nabla p) = 0 \quad . \tag{3.3}$$

If we try to upscale the absolute permeability for the elliptic pressure equation, we are dealing with a single-phase upscaling. The theory on single-phase upscaling is well analysed. We seek homogeneous block permeabilities on the coarse scale such that the single-phase flow is the same as on the fine scale. This is not trivial, and it causes problems when the media has a heterogenous structure since the heterogeneities at all scales have a significant effect on the coarse scale properties of the solution. It is therefore a difficult task to capture all the heterogeneities at the fine scale in the coarsened reservoir model.

In the long process it is to form a reservoir, the composite of different materials which was deposed varied in different period of times. As a respons to this process, different species of rock was deposed in layers on the bottom of the sea. Dramatic changes in the crust of the earth later resulted in hard species of rock surrounded the layered system and formed what we call a layered reservoir. The layers are characterized by different permeability.

We begin by a presentation of averaging the permeability in simple, layered heterogenous medium. In such geometries, we can find an average permebility K^* which will give an analytic correct answer on the scale of L and there are two fundamental types of averaging the permeabilty - harmonic averaging and aritmetic averaging. The power averaging procedure and other upscaling methods such as transmissibility upscaling and local- and global upscaling techniques for more general heterogenous medium will also be presented.

3.1.1 Harmonic Average

Assume that we have the situation given in Figure 3.1. Let the viscosity μ be constant, the fluid incompressible and consider one phase flow in one dimension. Darcy's law, Equation (2.7), where we have neglected the gravity force now becomes

$$u = -\frac{K(x)}{\mu} \frac{dp(x)}{dx} \quad . \tag{3.4}$$

In each volume, the permeability is changing in the x-direction. Since the fluid is incompressible, the velocity is constant. We can then define an average pressure gradient

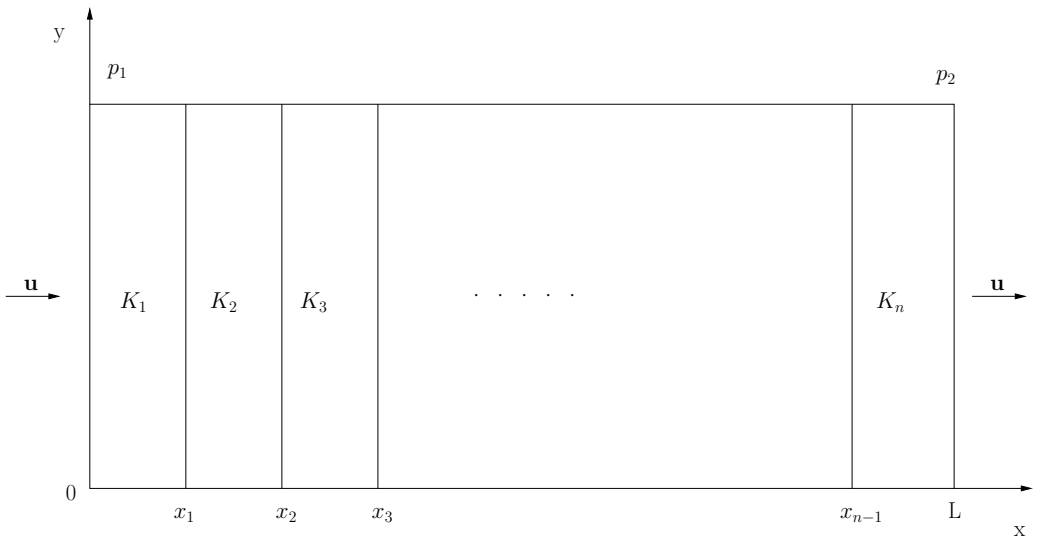

Figure 3.1: Averaging the permeability when the permeability-layers are orthogonal to the fluid flow.

$$\overline{\frac{dp(x)}{dx}} = \frac{p_2 - p_1}{L} \quad . \tag{3.5}$$

From Darcy law, we have

$$\frac{dp(x)}{dx} = -\frac{u\mu}{K(x)} \quad . \tag{3.6}$$

We can write

$$\int_{p_1}^{p_2} dp(x) = -u\mu \int_0^L \frac{1}{K(x)} dx \quad , \tag{3.7}$$

which gives

$$p_2 - p_1 = -u\mu \int_0^L \frac{1}{K(x)} dx \quad . \tag{3.8}$$

From the expression for the average pressure gradient, Equation (3.5), we can formulate

$$\overline{\frac{dp(x)}{dx}} = -\frac{u\mu}{L} \left(\int_0^{x_1} \frac{1}{K_1} dx + \int_{x_1}^{x_2} \frac{1}{K_2} dx + ... + \int_{x_{n-1}}^{L} \frac{1}{K_n} dx \right) \quad . \tag{3.9}$$

In last equation, we can define the harmonic average for the permeability

$$\frac{1}{K_H^*} = \frac{1}{L}\int_0^L \frac{1}{K(x)}dx \quad . \tag{3.10}$$

3.1.2 Arithmetic Average

Let us now consider the situation illustrated in Figure 3.2, and that the assumptions given in the harmonic average section also is applied here. Since the permeability now depends on the y-direction, Darcy's law can be written as

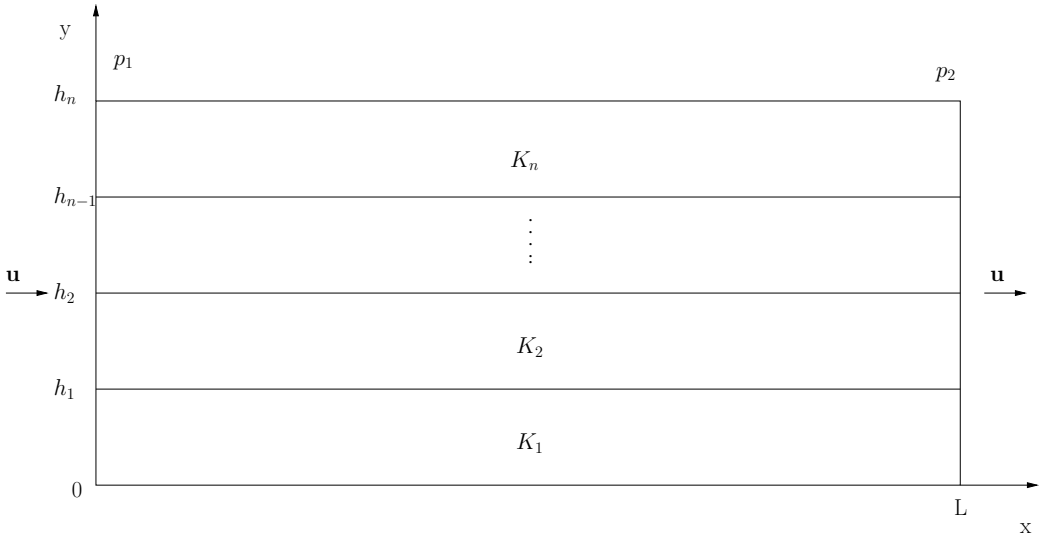

Figure 3.2: Averaging the permeability when the permeability-layers are parallel to the fluid flow.

$$u(y) = -\frac{K(y)}{\mu}\frac{dp}{dx} \quad . \tag{3.11}$$

Again we define an average pressure gradient

$$\overline{\frac{dp}{dx}} = \frac{p_2 - p_1}{L} \quad . \tag{3.12}$$

Note that Equation (3.12) doesn't vary in the x- or y-direction. By integrating Equation (3.11) over the length h_n, we get

$$\frac{1}{h_n}\int_0^{h_n} u(y)dy = -\frac{1}{\mu}\overline{\frac{dp}{dx}}\frac{1}{h_n}\int_0^{h_n} K(y)dy \tag{3.13}$$

$$= -\frac{1}{\mu}\frac{p_2-p_1}{h_n}\frac{1}{h_n}\left(\int_0^{h_1} K_1(y)dy + \int_{h_1}^{h_2} K_2(y)dy\right. \tag{3.14}$$

$$\left. +... + \int_{h_{n-1}}^{h_n} K_n(y)dy\right) \quad . \tag{3.15}$$

Now we can define the arithmetic average for the permeability

$$K_A^* = \frac{1}{h_n}\left(\int_0^{h_1} K_1(y)dy + \int_{h_1}^{h_2} K_2(y)dy + ... + \int_{h_{n-1}}^{h_n} K_n(y)dy\right) \quad . \tag{3.16}$$

3.1.3 Power Averaging Procedures

This method is based on power averaging of permeabilties at the fine scale. The power average of permeability components are defined by

$$K_i^* = \left(\frac{1}{V_b}\int_{V_b} K_i^{\eta_i} dV\right)^{1/\eta_i} \quad , \quad -1 \leq \eta_i \leq 1 \quad , \tag{3.17}$$

where V_b is the coarse block volume and both K^* and K are considered to be diagonal tensors. Note that when $\eta_i = 1$ or $\eta_i = -1$, we obtain the arithmetic and harmonic means respectively. By letting $\eta \to 0$, we will obtain the geometric mean given by

$$K_i^* = \exp\left(\frac{1}{V_b}\int_{V_b} \log[K_i]dV\right) \quad . \tag{3.18}$$

Actually, we can combine two values of η. If we for example have a stuctured layered system in the $x-z$ coordinate system, K_i^* can be computed by first harmonic averaging along each layer in the x coordinate direction and then by arithmetic averaging these layers averages in the z direction.

When we want to model porous media which is statistically homogeneous at the large scale, it is often beneficial to calculate the effective permeability K_e. We use the definition of K_e given in Durlofsky (14) saying that if the scale over which an averaged permeability is large relative to the of heterogenety within the porous medium, then the large scale is refered to as an effective permeabilty. Unfortunately, very often the conditions for the appearance of an effective permeability is not satisfied. The reason can be that the observed blocks are too small and hence there is no foundation to use a

statistical homogenous consept. As a respons, the equivalent permeability K_b in a volume V is defined due to Rubin and Gómez-Hernández (33) as

$$\frac{1}{V}\int_V \mathbf{u}\ dx = -K_b\frac{1}{V}\int_V \nabla p\ dx \quad . \tag{3.19}$$

An important property of the power averaging procedure is that it gives us a diagonal permeability tensor, while more general numerical methods described below will in most cases give a full tensor.

3.1.4 Local Calculation

The power averaging procedure described above has an unfortunate disadvantage - it lacks the generality for a numerical procedure. A more robust method for calcultating upscaled values for the permeability K^* and the transmissibility T^*, is to use a so-called local calculation. In order to use such methods, we must solve the pressure equation on the fine scale over the target coarse scale region. It can be profitable to include the effect of the neighbouring regions in these calculations. We then call the method an extended local procedure. Its advantage is that the effect from the boundary conditions are redused. We start by looking on some pure local methods.

A lot of local upscaling procedures use finite volume methods for the numerical calculations. When the fine scale permeability gives a diagonal tensor and the grid is othogonal, we can use the two-point flux approximation to get a finite difference scheme for the numerical solution. Otherwise, if the permeability on the fine scale results in a full tensor and the grid is non-orthogonal, multipoint flux approximation is the method we should use.

3.1.5 Boundary Conditions

The impose of boundary conditions in local methods are important to discuss. Unfortunately, the dependency on the boundary conditions may introduce large errors in the coarse scale model. What kind of boundary conditions one should use, is likely to be case dependent. We will here look on two categories of boundary conditions, fixed pressure boundary conditions and periodic boundary conditions. Figure 3.3 will be used as an illstration.

Fixed Boundary Conditions

For the fixed pressure boundary condition, the simplest way to give boundary conditions are with a constant pressure and no flow boundary specification.

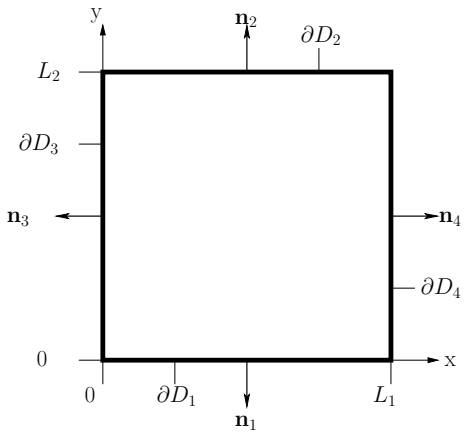

Figure 3.3: A domain used for fixed- and periodic boundary condition.

With reference to Figure 3.3, fixed boundary conditions can be specified for flow in the x-direction as follows,

$$p(0, y) = 2 \tag{3.20}$$

$$p(L_1, y) = 1 \tag{3.21}$$

$$\mathbf{u}(x, 0) \cdot \mathbf{n}_1 = -\mathbf{u}(x, L_2) \cdot \mathbf{n}_2 = 0 \quad . \tag{3.22}$$

We let the pressure difference be given in the y-direction in the second solution. The equations above mean that we only allow the fluid to flow between the vertical or the horizontal lines in an orthogonal grid for example. The difference in pressure is the only reason why the fluid flow. After we have solved the elliptic pressure equation with the boundary conditions given above in x- and y-direction, we can compute the total flow rates through the target coarse block. The total flow rate in the x-direction is given by the following equation

$$q_1 = \int_0^{L_2} \mathbf{u}(L_1, y) \cdot \mathbf{n}_4 dy = \sum_{l=1}^{N_f} (\mathbf{u}_l \cdot \mathbf{n}_4) \Delta y_l \quad , \tag{3.23}$$

where N_f is the number of fine cells in the y-direction and Δy is the thickness of cells in the y-direction. q_2 can be computed in the same manner. Assuming that μ is a constant and using Darcy's law in 1D over the length of the target block in the x-direction, we get

$$\mathbf{u} = -K_1^* \frac{dp}{dx} = -K_1^* \frac{\Delta p}{L_1} \quad . \tag{3.24}$$

By the definition of flow rate and that we have a 1D-problem ($A = L_2 * \Delta z$, where we put $\Delta z = 1$), we will have that

$$q_1 = \mathbf{u} \cdot A = -K_1^* \frac{\Delta p}{L_1} \cdot L_2 \quad . \tag{3.25}$$

This implies when $\Delta p = 1$ that

$$K_1^* = -\frac{q_1 L_1}{L_2 \Delta p} = -\frac{q_1 L_1}{L_2} \quad . \tag{3.26}$$

The same procedure is done for the calculation of K_2^*. We will get a diagonal tensor if we are using such boundary conditions on an orthogonal grid. Such boundary conditions have been used in this thesis.

If we use fixed boundary conditions in order to upscale the permeability K, we will in general not get an symmetic tensor. Another drawback with no flow boundary conditions is that we do not permit the calculation of a full tensor K^* via integration over boundaries. By computing volume averaged velocites and pressure gradients over the entire flow domain, we can enforce symmetry and positive definiteness for K^*. There are several ways of specifying the fixed boundary conditions, and an alternative, which is more general, is to use boundary conditions that specify a linear pressure variation along the sides parallel to direction of the pressure gradient. A linear pressure variation is used in the full tensor calculation in Section 3.1.6. Using linear pressure variation in geological models are done in King and Mansfield (28).

Periodic Boundary Conditions

When using periodic boundary conditions, we need to solve two local fine scale problems for a 2D-system. One for each coordinate direction. We assume that the system is replicated periodically in space and that the global pressure can be approximated on the scale of x^* as $p = p_0 + \mathbf{G} \cdot (x^* - x_0^*)$, where $\mathbf{G} = G_1 \mathbf{i}_1 + G_2 \mathbf{i}_2$ is a constant vector. Such boundary conditions may be given as follows, with reference to Figure 3.3,

$$p(x,0) = p(x,L_2) - G_2 L_2 \qquad \text{on} \quad \partial D_1 \quad \text{and} \quad \partial D_2 \tag{3.27}$$

$$p(0,y) = p(L_1,y) - G_1 L_1 \qquad \text{on} \quad \partial D_3 \quad \text{and} \quad \partial D_4 \tag{3.28}$$

$$\mathbf{u}(x,0) \cdot \mathbf{n}_1 = -\mathbf{u}(x,L_2) \cdot \mathbf{n}_2 \qquad \text{on} \quad \partial D_1 \quad \text{and} \quad \partial D_2 \tag{3.29}$$

$$\mathbf{u}(0,y) \cdot \mathbf{n}_3 = -\mathbf{u}(L_1,y) \cdot \mathbf{n}_4 \qquad \text{on} \quad \partial D_3 \quad \text{and} \quad \partial D_4 \quad . \tag{3.30}$$

Periodic boundary conditions guarantee that the resulting K^* will be symmetric and positive definite. An example where the author is using periodic boundary condition can be found in Bøe (6). He has applied and

analyzed a scaling method based on conservation of dissipation with periodic and symmetric boundary conditions. Durlofsky (14) treats a periodic system for the calculation of an effective permeability. With such a system, it is natural to use periodic boundary conditions. For examples of periodic boundary conditions used in describing flow in porous media, see Durlofsky and Brady (18).

3.1.6 Full Tensor Calculation

In this thesis, we are calculating a full permeability tensor by using fixed pressure boundary conditions and a linear pressure variation in order to compare the result with a diagonal tensor. We want to solve the elliptic pressure equation, Equation (3.3), on an orthogonal grid. In the x-direction, we use the following conditions with reference to Figure 3.3

$$p(0, y) = 2 \tag{3.31}$$
$$p(L_1, y) = 1 \tag{3.32}$$
$$p(x, 0) = p(x, L_2) = 1 - \frac{x}{L_1} \quad . \tag{3.33}$$

We specify the conditions in the y-direction as follows

$$p(x, 0) = 2 \tag{3.34}$$
$$p(x, L_2) = 1 \tag{3.35}$$
$$p(0, y) = p(L_1, y) = 1 - \frac{y}{L_2} \quad . \tag{3.36}$$

As mentioned in Section 3.1.5, no flow boundary condition do not permit caluculation of a full tensor K^* via intergration over boundaries. By computing volume averaged velocities and pressure gradients over the entire flow domain, we will demonstrate the calculating of a full tensor. The following equations are used to compute averaged velocities and pressures

$$\overline{\mathbf{u}^j} = \frac{1}{V_{b,l}} \int_V \mathbf{u}^j dV = \frac{1}{V_b} \sum_{l=1}^{N_t} \mathbf{u}_l V_{b,l} \quad , \tag{3.37}$$

$$\overline{\nabla p^j} = \frac{1}{V_b} \int_V (\nabla p)^j dV = \frac{1}{V_b} \sum_{l=1}^{N_t} (\nabla p)_l V_{b,l} \quad , \tag{3.38}$$

where $j = 1$ results in a flow solution with pressure difference in the x-direction and $j = 2$ gives the flow solution with pressure difference in the y-direction. The sumation are is taken over all N_t fine blocks that cover the coarse target block and $V_{b,l}$ indicates the bulk volume of fine scale cell l. In the MATLAB-program that we have been using, we have max $N_t = 80$. $\overline{\mathbf{u}}$ and $\overline{\nabla p}$ have two components since it is a two dimensional problem. Further, since we solve two flow problems, we can compute four components of K^* from the two solutions. From Darcy's law, we get the following set of equations

$$\overline{u_1^1} = -(K_{1,1}^* \overline{\nabla p_1^1} + K_{1,2}^* \overline{\nabla p_2^1}) \tag{3.39}$$
$$\overline{u_2^1} = -(K_{2,1}^* \overline{\nabla p_1^1} + K_{2,2}^* \overline{\nabla p_2^1}) \tag{3.40}$$
$$\overline{u_1^2} = -(K_{1,1}^* \overline{\nabla p_1^2} + K_{1,2}^* \overline{\nabla p_2^2}) \tag{3.41}$$
$$\overline{u_2^2} = -(K_{2,1}^* \overline{\nabla p_1^2} + K_{2,2}^* \overline{\nabla p_2^2}) \quad , \tag{3.42}$$

where the subscript indicates the vector component and the superscript the flow problem. We can rearrange the set of equations to give a matrix equation

$$\begin{pmatrix} \overline{\nabla p_1^1} & \overline{\nabla p_2^1} & 0 & 0 \\ 0 & 0 & \overline{\nabla p_1^1} & \overline{\nabla p_2^1} \\ \overline{\nabla p_1^2} & \overline{\nabla p_2^2} & 0 & 0 \\ 0 & 0 & \overline{\nabla p_1^2} & \overline{\nabla p_2^2} \end{pmatrix} \begin{pmatrix} K_{1,1}^* \\ K_{1,2}^* \\ K_{2,1}^* \\ K_{2,2}^* \end{pmatrix} = - \begin{pmatrix} \overline{u_1^1} \\ \overline{u_2^1} \\ \overline{u_1^2} \\ \overline{u_2^2} \end{pmatrix} \quad , \tag{3.43}$$

which we can solve and find the components of K^*. There are many methods we can use in order to make the K^* computed by Equation (3.43) symmetric. It is for example possible to apply a least square problem. In our program, we enforce symmetry by simply applying $K_{1,2}^* - K_{2,1}^* = 0$. Equation (3.43) then becomes

$$\begin{pmatrix} \overline{\nabla p_1^1} & \overline{\nabla p_2^1} & 0 & 0 \\ 0 & 0 & \overline{\nabla p_1^1} & \overline{\nabla p_2^1} \\ \overline{\nabla p_1^2} & \overline{\nabla p_2^2} & 0 & 0 \\ 0 & 0 & \overline{\nabla p_1^2} & \overline{\nabla p_2^2} \\ 0 & 1 & -1 & 0 \end{pmatrix} \begin{pmatrix} K_{1,1}^* \\ K_{1,2}^* \\ K_{2,1}^* \\ K_{2,2}^* \end{pmatrix} = - \begin{pmatrix} \overline{u_1^1} \\ \overline{u_2^1} \\ \overline{u_1^2} \\ \overline{u_2^2} \\ 0 \end{pmatrix} \quad . \tag{3.44}$$

3.1.7 Transmissibility Upscaling

If we have found a solution from the fine grid, we can compute the transmissibilities by averaging over coarse block regions and then apply the following equation with reference to Figure 3.4

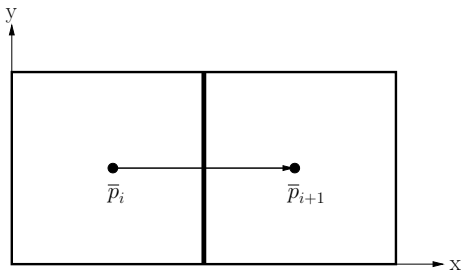

Figure 3.4: A domain used for transmissibility upscaling.

$$(T)_{i+\frac{1}{2}} = \frac{(q_1)_{i+\frac{1}{2}}}{\overline{p}_i - \overline{p}_{i+1}} \quad , \tag{3.45}$$

where $\overline{p}_i$ is the average pressure over the region corresponding to coarse block i and $(q_1)_{i+\frac{1}{2}}$ is the flow rate across the interface $i+\frac{1}{2}$. Since calculated upscaled permeability tensors are only used in finite difference reservoir simulators in order to find the transmissibilities, many upscaling procedures are focusing on transmissibility calculation in stead of calculating a permeabilty tensor. The equations that calculate the transmissibility when upscaled permeabilities are known, is given by

$$(T_x)_{i+\frac{1}{2}} = \frac{2(K_x^*)_{i+\frac{1}{2}}\Delta y \Delta z}{\Delta x_{i+1} + \Delta x_i} \tag{3.46}$$

where

$$(K_x^*)_{i+\frac{1}{2}} = \frac{(\Delta x_{i+1} + \Delta x_i)(K_x^*)_i (K_x^*)_{i+1}}{\Delta x_{i+1}(K_x^*)_i + \Delta x_i (K_x^*)_{i+1}} \quad . \tag{3.47}$$

Δx,Δy and Δz indicate the size of the grid blocks at their respective coordinates.

Chen et al. (9) have developed and applied a technique for calculating coarse scale permeability and transmissibility properties for highly heterogensous models. In highly heterogenous models, the transmissibilities may be negative. Therefore we need to iterate until all of the transmissibilities are positive and a level of accordance between the fine and the coarse solutions are achieved.

3.1.8 Global Calculation

In most global upscaling techniques, we must first solve a global fine scale flow problem and then use information from this solution to extract coarse scale quantities. The disadvantage with a global calculation, is that we need to run a global fine scale simulation first. There are indeed global upscaling techniques where we do not need to run a fine scale simulation, see for example Chen and Durlofsky (8). The idea in global upscaling methods, is to minimize errors of flow between the fine and the coarse scale. In order to reduce the error, we need to iterate until an acceptable result is achieved. In many global upscaling techniques, it is usual to apply transmissibility upscaling for the calculation of coarse grid quantities instead of the permeability. In most cases, this will give a more stable procedure.

The general global upscaling algorithm first calculates the average pressure $\overline{p}$ and the flow rate q_j, $j = 1, 2$ for a two dimensional problem, on the fine grid. Next, it is usual to use this information on the coarse grid. In order to transfer the information from a fine to a coarse scale, projection methods are often used. Then we calculate the transmissibility on the coarse scale by using Equation (3.45). The last step is then to minimize the transmissibility error on the coarse scale to be as small as possible by calculating new transmissibilities with other values for $\overline{p}$. This iteration procedure will continue until we have found an acceptable transmissbility at the coarse scale.

It is important to be aware of that global upscaling techniques are not stable under large boundary value changes. The reason is that global upscaling investigates regions of the reservoir with flow. By that reason, some regions are badly or sometimes not determined at all. By changing the boundary conditions, we get new flow pattern and flow into not investigated regions which can result in an unstable upscaling procedure.

Many global upscaling procedures first solves the pressure equation at the measurment scale, and then use the average flow criteria, Equation (3.19), in order to get a block conductivity tensor. Unfortunately, we will not get as many equations as we need in order to determine a full non-diagonal conductivity tensor. Holden and Nielsen (26) solve this problem by seeking coarse grid finite difference transmissibilities, without calculating block conductivety tensors. Then one global fine pressure computation would be enough to get all the information we need for a single-phase reservoir simulation. In a local upscaling technique, a fine scale problem is solved for each target coarse block. The time a local procedure needs to compute fine scale problems on target coarse blocks, is comparable to solve a global fine scale pressure equation. By computing a fine scale pressure, they can compare the fine and coarse scale pressure and velocity. They show that by minimizing a

L_2 norm defined as

$$\|p_{fine} - p_{coarse}\|_{L_2}^2 = \int_V (p_{fine} - p_{coarse})^2 dx \tag{3.48}$$

$$\|\mathbf{u}_{fine} - \mathbf{u}_{coarse}\|_{L_2}^2 = \int_{\delta V} [(\mathbf{u}_{fine} - \mathbf{u}_{coarse}) \cdot \mathbf{n}]^2 dx \tag{3.49}$$

we obtain a good upscaling procedure.

3.2 Two-Phase Upscaling

If we assume that we have an immiscible, incompressible two-phase flow, i.e. oil and water, in a heterogeneous media, it can be described by Darcy law, the mass-conservation law and the saturation equation for the wetting phase, see Chapter 2 and Section 2.3.3. The critical point from a numerical point of view, is that the pressure- and the saturation equations are coupled together through the saturation dependence in phase mobilities

$$\nabla \cdot (K\lambda(S) \cdot \nabla p) = q \quad . \tag{3.50}$$

The connection is non-linear and makes two-phase flow in heterogenous porous media to a challenging problem. In one-phase upscaling procedures, the upscaling of absolute permeability is in many cases enough to give a good representation of the fine scale model at a coarse scale. This is not the case for two-phase upscaling problems. Here we must also incorporate the large scale effect of the relative permeability in addition to capture the macroscopic effect of absolute permeability. This is in general a difficult problem to model since we must reflect the sharpe hyperbolic saturation front and also capture the small flow channels on the coarse grid.

3.2.1 Pseudo-relative Permeability Functions

In many years the use of pseudo-relative permeability curves, or pseudo functions, was the way to handle this upscaling problem. The main target in such methods are to avoid numerical dispersion. Pseudo functions are constructed such that, by modifying the fine scale relative permeability curves, they account for geological heterogenities on the coarse grid. The idea is to predict the flow rate of each phase out of the coarse grid blocks as the water flood progresses in time throughout the simulation run. Hence pseudo-relative permeabiltiy curves are different in each coarse block. In order to calculate the upscaled relative permeability, we must specify the saturation at the inlet of

the coarse block and the pressure or flux must be given on each boundary. This approach depends therefore on the boundary and initial conditions, the flow field and parameters defined for a fine scale simulation.

In general, the use of pseudo-function has been critized for being unreliable and limited to cases where capillary or gravity equilibrium can be assumed at the coarse level, see Barker and Thibeau (4).

3.2.2 Averaged Equations

As a respons to the pseudo-function method, researchers have developed methods with volume averaged equations where the idea is to denote the unknown quantities in terms of average and fluctating components or moments. Let us assume that we have a fine grid region defined on a target coarse block in a x-y coordinate system. For any variable $\Phi(x, y)$, we can write

$$\Phi(x, y) = \overline{\Phi} + \widetilde{\Phi}(x, y) \quad , \tag{3.51}$$

where the overbar indicates a constant volume averaged quantity and the tilde is a spartially varying fluctating quantity. In two dimension, the volume average is given by

$$\overline{\Phi} = \frac{1}{A} \int_D \Phi(x, y) dA \quad , \tag{3.52}$$

where D denotes the coarse grid region and A the area of the region. If we use this concept, we can define

$$S(x, y) = \overline{S} + \widetilde{S}(x, y) \tag{3.53}$$

$$\mathbf{u} = \overline{\mathbf{u}} + \widetilde{\mathbf{u}}(x, y) \tag{3.54}$$

$$\overline{f} = \frac{1}{A} \int_D f(S(x, y)) dA \tag{3.55}$$

$$\widetilde{f}(S(x, y)) = f(S(x, y)) - \overline{f} \quad . \tag{3.56}$$

By inserting these equations into Equation (2.13) where we put $\epsilon = 0$, we get

$$\frac{\partial \overline{S}}{\partial t} + \frac{\partial \widetilde{S}}{\partial t} + \overline{\mathbf{u}} \cdot \nabla \overline{f}(S) + \overline{\mathbf{u}} \cdot \nabla \widetilde{f}(S) + \widetilde{\mathbf{u}} \cdot \nabla \overline{f}(S) + \widetilde{\mathbf{u}} \cdot \nabla \widetilde{f}(S) = 0 \quad . \tag{3.57}$$

By averaging Equation (3.57) and note that averages over single primed terms are zero, the coarse scale two-phase flow then take the form of an average saturation equation

$$\frac{\partial \overline{S}}{\partial t} + \overline{\mathbf{u}} \cdot \nabla \overline{f}(S) + \overline{\widetilde{\mathbf{u}} \cdot \nabla \widetilde{f}(S)} = 0 \tag{3.58}$$

and a sequence of moment equations

$$\frac{\partial \widetilde{S}}{\partial t} + \overline{\mathbf{u}} \cdot \nabla \widetilde{f}(S) + \widetilde{\mathbf{u}} \cdot \nabla \overline{f}(S) + \widetilde{\mathbf{u}} \cdot \nabla \widetilde{f}(S) = \overline{\widetilde{\mathbf{u}} \cdot \nabla \widetilde{f}(S)} \quad . \tag{3.59}$$

We have in both cases neglected the gravity and capillary pressure and assumed the porosity to be a constant. By using the volume averaged equations as a framework, Durlofsky (16) discusses the assumptions, strengths and limitations for the use of pseudo-functions, a nonuniform coarsing of the fine grid model and the use of higher moments of the fine scale variables.

3.2.3 Averaged Equations in a Stochastic Context

The paper by Langlo and Espedal (29) is an example where they use the averaged saturation and moment equations in the context of a stochastic method. The permeability is given as a log-normal random function with a given mean, variance and correlation. Choosing the permeability as a log-normal random function is usually a reasonable assumption due to Sudicky (37) and Freeze (24). They have further assumed that the flow is incompressible and neglected the gravity forces. In the paper, they present two averaged saturation equations - with and without capillary forces. We will only present the method without capillary forces. The saturation they are working with is given by Equation (2.13) in Chapter 2. For small values of ϵ, the saturation equation is almost hyperbolic and dominated by the convective part,

$$\phi \frac{\partial S}{\partial t} + \nabla \cdot (f(S)\mathbf{u}) = 0 \quad . \tag{3.60}$$

Since the conventional flow function will give a shock solution after some time, they split this function in two parts,

$$f(S) = H(S) + b(S)S \quad , \tag{3.61}$$

where $H(S)$ is given as

$$H(S) = \begin{cases} \frac{f(S_{BL})}{S_{BL}} \cdot S & \text{if } 0 \leq S \leq S_{BL} \\ f(S) & \text{if } S_{BL} < S \leq 1 \end{cases} \tag{3.62}$$

where S_{BL} is the Buckley-Leverett shock saturation. The terms $H(S)$ and $b(S)S$ are the convection and the diffusion part of the fractional flow function, respectively. They define the random saturation as

$$S = \widehat{S} + \widetilde{S} \quad , \tag{3.63}$$

where $\widehat{S}$ denotes the expected saturation and $\widetilde{S}$ are the fluctuations. Further, the random velocity is given in the same manner

$$\mathbf{u} = \widehat{\mathbf{u}} + \widetilde{\mathbf{u}} \quad , \tag{3.64}$$

By inserting the equations above in Equation (3.60), the solution is described by

$$\frac{\partial}{\partial t}(\widehat{S} + \widetilde{S}) + \nabla \cdot [f(\widehat{S} + \widetilde{S})(\widehat{\mathbf{u}} + \widetilde{\mathbf{u}})] = 0 \quad . \tag{3.65}$$

Since we have assumed $\epsilon = 0$, the saturation equation is convection dominated and hence the diffusion correction part is neglected. By a Taylor-expansion in terms of $\widehat{S}$ and $\mathbf{u}$, they arrive approximated solution equation. It is assumed that $F''(S) \equiv 0$ when $S < S_{BL}$ and for $S > S_{BL}$ they state that $F''(S) \approx 0$ and that ∇S vary slowly. Finally by taking the expected value of the calculated equation, they show that the equation can be written as

$$\frac{\partial}{\partial t}(\widehat{S}) + \nabla \cdot [F(\widehat{S})\mathbf{u}] + \nabla \cdot [F'(\widehat{S})\widetilde{S}\widetilde{\mathbf{u}}] = 0 \quad . \tag{3.66}$$

An expression for the covariance $\widetilde{S}\widetilde{\mathbf{u}}$ is needed and the details in order to acheive this expression is obmitted here.

It is demostrated in the paper that the average saturation solution for a stochastic system gives a very accurate approximation of the flow. They compare their macrodispersion solutions with high-resolution solutions of the original equations based on several types of permeability fields. One of the disadvantages with a fully stochastic approach is that it can be difficult to implement additional effects in the model without a significant reformulation.

3.2.4 Averaged Equations in a Deterministic Framework

We begin this section by mention that in Durlofsky (15), the first successful attempt to use volume averaged equations in a deterministic framework is presented. This means that the permeability distributions are fully specified. Many of the existing volume-based upscaling procedures of two-phase flow, neglects the saturation dependence in the pressure equation and specify a unit mobility ratio instead. In the work of Efendiev and Durlofsky (19), this

problem has been taking into account and they demonstrate promising results. As in many cases when it comes to volume-based upscaling procedures, they have neglected the gravity and the capillary forces.

3.2.5 Combined Averaged Equations

The findings from the stochastic frameworks are taken into account and further developed in Efendiev and Durlofsky (20). In this paper, they consider deterministic systems and apply numerical techinques in order to develop a coarse scale saturation equation. The coarse scale saturation equation they present is a non-linear convection-diffusion equation, given by

$$\frac{\partial S^*}{\partial t} + \nabla \cdot G^*(x, S^*) = \nabla \cdot D^*(x, S^*) \nabla S^* \quad , \tag{3.67}$$

where the coarse scale flux function can be written as

$$G^*(x, S^*) = \mathbf{u}^* f(S^*) + m^*(x, S^*) \quad . \tag{3.68}$$

The star indicates a coarse scale parameter, D^* and m^* are the coarse scale diffusive and convective correction, respectively. The convection-diffusion equation is motivated by previous results which they discuss in the paper. $D^*(x, S^*)$ and $m^*(x, S^*)$ are calculated from local fine problems, and they present two procedures for the determination of those parameters. They call the two methods loosely and tightly coupled models and differ mainly in the boundary conditions applied for determination of D^*. The model has been applied to examples involving heterogeneous fields and different global boundary conditions with good results.

3.3 Hierarchy Upscaling

A special focus in this thesis will be on so-called hierarchy upscaling methods. The idea in such an approach is to use the fact that fractures vary over multiple length scales. Fractures that are very short will affect the flow in a grid block to a much smaller degree than fractures with lengths of the order of the grid block size. Therefore it is common to seperate the fracture network in seperate scales due to the size, intensity and orientation of the fractures. Many researchers use a three-level scale where the fracture network is distributed on a large-, intermediate- and fine scale.

3.3.1 Approaches on a Three-Level Scale

Lee et al. (30) have used this three-level scale in order to model flow in a naturally fractured reservoir with multiple length scale fractures. First they choose a grid size for the reservoir, and then they divide all fractures in three categories - large, medium and short fractures. The method is in other words based on the sizes of geological structures relative to the grid cells. They demonstrate a method for calculating the effective conductivity contribution from each scale level. The results that come from short fractures are used as an effective matrix permeability for the next scale computation of an effective grid block permeability. The long fractures are modeled explicitly as a considerable fluid channel and can be treated as a well in a reservoir simultion formulation. The method is based on the hypothesis of equivalent property approximation for simulation grid blocks. Their method is an efficent procedure for modeling fractures of multiple lengths. It is to believe that if the length scale distribution is uniformely distributed, the approximation will give less accurate results.

Another hierarchy approach based on a three-level scale, can be found in Berg and Øian (5). A series of two-phase flow simulation experiments are presented on four geological cases. All the structures consist of lower permeability fault rocks in a high permeability host rock. The simulation runs show that each scale has a considerable effect on the saturation, pressure drop and oil production. Their results indicate the importance of the scale-dependency when we analyze the effect of faults in two-phase flow.

3.4 The Domain Decomposition Method

In the domain decomposition method, we try to split the original problem into smaller tasks. The physical domain is divided into subdomains which may or may not overlap. The overlap is represented by a parameter $\delta = 0$. Then the original problem can be reformulated as an iterative process over local subproblems. This process is coupled together through the boundary values in the local problems. Well-known domain decomposition methods are the classical Schwarz method and the Galerkin method. The classical Schwarz method and other domain decomposition algorithms which use a multiscale finite element method for the coarse subdomain correction, can be found in Aarnes (1). In order to speed up the iterative process, we can use a precondition method. If we say that L_1 defines the length of the coarse block and l_1 the length of every fine grid cell in a uniform 2D-model ($L_1 = L_2$ and $l_1 = l_2$), we know that the number of iterations for a domain decomposition

method are proportional to $\frac{1}{L_1}$. Further, if $\frac{\delta}{L_1}$ gives a constant value, then the number of iteration steps are independent of L_1 and $\frac{l_1}{L_1}$. If $\delta = 0$, then we know that the iteration process is slow and all the local upscaling methods can be applied. The number of iteration steps will decrease by using $\delta > 0$.

3.4.1 A Method Based on Domain Decomposition

The idea to seperate fractures in different scales, led researches to the idea of representing the permebility in such a way too. By using the simplicity of the Haar system, it gives a permeability representation which is consistent with a domain decomposition method. In the paper by Hersvik and Espedal (25), they want to upscale the absolute permeability and represent values of absolute permeability as different levels with the Haar system as hierarchical basis functions. This leads to a wavelet representation of the permeability. Results in their paper which are based on two-phase flow in a heterogeneous reservoir with a quarter of a five-spot problem, show that the dissipation and the mean velocity is conserved well. Further they present a theorem on a posteriori error estimate for velocity and pressure. Given a high level in the hierarchy model means that all scales in the permeability are represented. On the other side, we will have a low level model if the permeability is given as a global mean over different scales. By dividing the models in such a manner, we obviously need a criterion to select the "correct" level. A theorem and proof about such a criteria, can be found in Hersvik and Espedal (25, p.315-320).

Chapter 4

The Geometry and Petrophysical Properties of a Fault Damage Zone

If the permeability changes with the position, we say that the media is heterogenous. In order to capture the heterogeneties in reservoirs, faults need to be taken into account. Since they occur on all scales it is a difficult task to discretize and do numerical simulations for faulted reservoirs. In this chapter, we will describe typical geological properties of faulted and fractured porous media which will effect the numerical simulations. A special focus will be on the so called damage zone which we will model in this thesis.

4.1 Definitions and Concepts of Fractures and Faults

In this section we will give a brief overview of some of the fundamental concepts and terminology of fractures and faults. Further information regarding these issues can be found in Davies and Reynolds (13) and Marshak (31).

During a brittle deformation induced by tectonic stress for example, a material breaks into two or more pieces. The geological structures that are products of brittle deformation are in general called fractures. They form a discontinuity in rocks. These structures are possible to classify in different types due to their formation conditions and appearance, i.e. joints, faults and shear band. Faults are defined as a fracture on which slip or sliding occurs. Most faults have a slope, and the mass of rock above a sloping fault plane is referred to as the hangingwall, see Figure 4.1. The mass of rock below the fault plane, is called the footwall.

A fault can be characterized by its strike- and dip angle, see Figure 4.1, and by its displacement and throw. We define the displacement to be the amount of slip along the fault. We can seperate different types of faults due to this concept as for example normal, reverse and strike-slip. A normal fault is formed when the hanging wall slips down the slope of the fault, and a reverse fault when the hanging wall slips up the slope. Dip-slip faults are a particular class of normal faults, and normal faults occur quite frequently in tensional regimes and are found for example in North Sea reservoirs. We will in this thesis focus on normal faults.

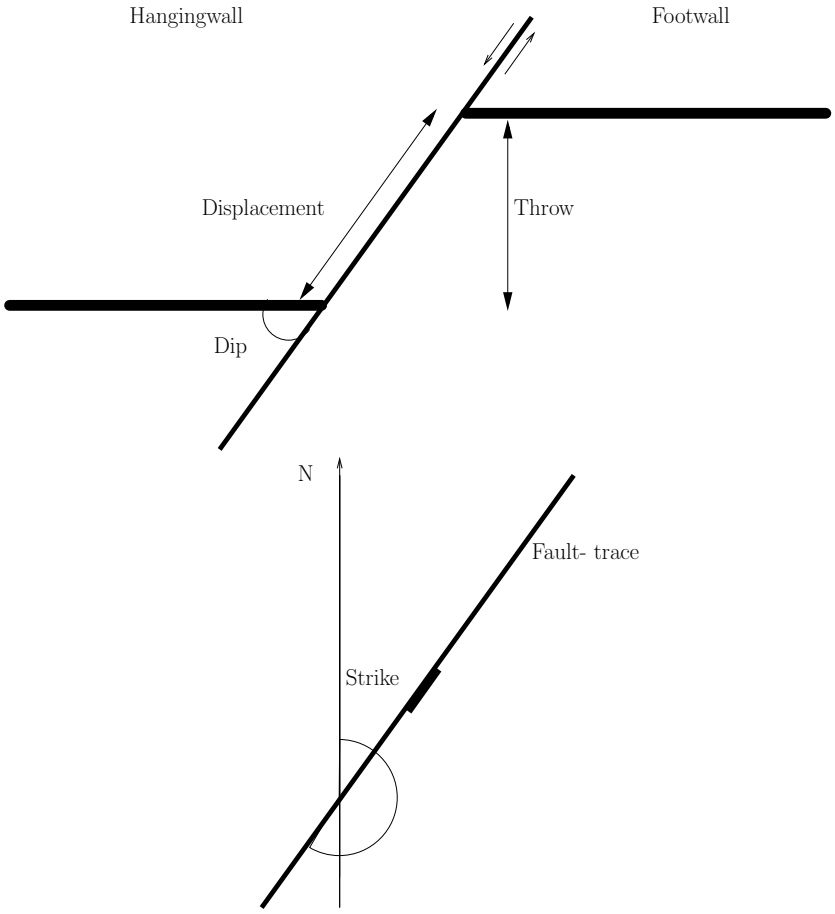

Figure 4.1: A figure illustrating some characteristics of normal fault zones in a vertical (top figure) and a horizontal (bottom figure) plane.

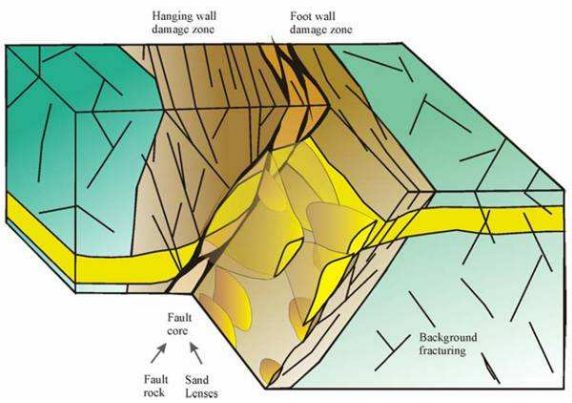

Figure 4.2: This figure shows the damage zone (brown) and the fault core (orange). Modified from Alvar Braathen, 2004.

4.2 The Main Architecture of Normal Faults

Fracturing occurs on several length scales within a fault zone. Therefore fault zones are composed of distinct components, and we will in this section use the fault zone architecture given by Caine et al. (7). They divide the fault zone in two - a fault core where most of the displacement is accommodated and in an associated damage zone that is mechanically related to the growth of the fault. See Figure 4.2. A fault core may include rock lenses, slip surfaces, gouge, cataclastic and mylonite. The variation in thickness within a fault core strongly influence the control of fluid flow properties. This thesis aims mainly to represent a damage zone. According to Caine et al. (7), a damage zone is the network of subsidary structures for example small faults, fractures, veins and folds, that bound the fault core. The rocks are less deformed than in the core, so the permeability is close to the one of the host rock. Wide damage zones may indicate multiple episodes of dip. It can be mentioned that geologist do not agree where to define exactly the boundary between the fault core and the damage zone. In Figure 4.3 we can see the fracture frequency as a function of the distance from the fault core. It shows that the frequency decreases away from the fault core.

4.3 Deformation Bands

Deformation bands are the most common strain localization features in damage zones in deformed porous media such as sandstones. In this section we will state the characteristics and petrophysical properties of deformation

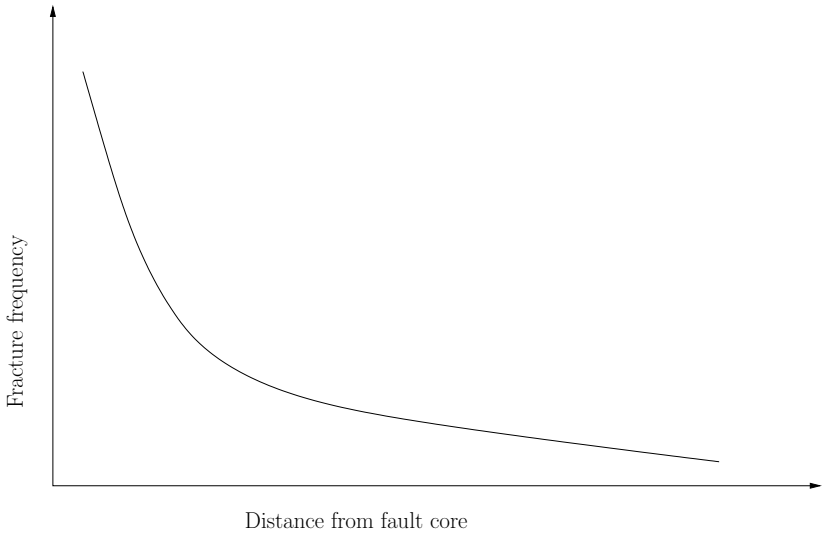

Figure 4.3: The fracture frequency as a function of the distance from the fault core.

bands. We will also discuss the connection between deformation bands, faults and damage zones. For a more detailed summary on deformation bands, the paper by Fossen et al. (23) is recommended.

We have studied damage zone in a porous media. So, in that case, the main secondary structures in the damage zone are deformation bands. In porous rocks, deformation bands are low-displacement deformation zones of thickness up to a few millimeters and a displacement up to a few centimeters. They have often a much stronger cohesion and also a reduced permeability compared with the host rock. We can find deformation bands in clastic reservoirs and aquifers, and they should deserve attention due to their potensial influence to fluid flow. If deformation bands act as real barriers to fluid flow is still controversial, and we refer to the paper by Fossen and Bale (22) for a discussion about this. Another reason for studying deformation bands are, from a geological point of view, that they provide information about the unique way that faults form in porous sandstones and on progressive deformation in porous media in general.

4.3.1 Characteristics of Deformation Bands

Here we follow the categorization which has been done in Fossen et al. (23). They summarize the characteristics of deformation bands as follows

- Deformation bands are restricted to porous granular media, notably

porous sands and sandstones.

- A deformation band does not represent a slip surface.
- Deformation bands occur hierarchically as individual bands, as zones of bands, or within zones associated with slip surfaces.
- Individual deformation bands rarely host offsets greater then a few centimeters even when the bands themselves are 100 meter long.
- Deformation bands are found in many upper-crustal tectonic and non-tectonic regimes.

4.3.2 The Difference between Deformation Bands and Slip Surfaces

There are several important characteristics that distinguish deformation bands from slip surfaces. The differences in mechanical evolution and structual expression may significantly influence fluid flow and therefore have direct implications for the management of the porous hydrocarbon and groudwater reservoirs in which they are very likely to occur. Deformation bands are thicker and exhibit smaller offsets than classical slip surfaces of comparable length. Whereas cohesion is lost and reduced across ordinary fractures, most deformation bands maintain or even increase cohesion. Finally, deformation bands often exhibit reduction in porosity and permeability, whereas both slip surfaces and tension fractures are typically associated with a permeability increase.

4.4 The Importance of Fault Damage Zones in Fluid Flow

In this thesis we will develop a numerical model based on damage zones of extensional faults in silicicalstic sediments. The geometry of the models will be based on field data.

4.4.1 Deformation Bands' Effect on Fluid Flow

Permeability measurements across deformation bands have led many researchers to conclude that deformation bands reduce transmissibility in a reservoir. It can be shown that the majority of deformation bands show

some reduction in permeability, some by as much as several order of magnitude. There are cases where deformation bands appear to be conduits for fluids. The influence of deformation bands on fluid flow depends on their internal permeability relative to the surrounding rock and their practical effect on fluid flow is still a matter of debate, see Fossen and Bale (22). For two phase flow, capillary pressure becomes relevant. In hydrocarbon reservoirs the capillary threshold pressure of the fault rock determines how much i.e. oil can accumulate on one side of the fault before across-fault migration occurs. Calculation predict that deformation bands cannot hold much more than a 20 meter or perhaps up to 75 meter high column of hydrocarbons. The practical consequence of deformation bands depends on other factors than permeability contrasts. Their continuity or variation in thickness and permeability in three dimensions is critical.

Chapter 5

The Numerical Model

In this chapter we will describe how we developed the numerical model. We have used commercial reservoir tools, Irap RMS and Havana Robusto, for this purpose. For the simulation part of the work, we have used Eclipse.

5.1 The Drawback of Commercial Reservoir Software

There is a lot of on-going research focusing on constructing reservoir simulators trying to describe fluid flow in porous media. In the industry, it is common to use commercial reservoir softwares. In commercial reservoir tools, the Central Processing Unit (CPU) limitation causes bigger problems due to a more user-friendly software which will result in a program code containing unnessaccary information. This will from a practical point of view mean that only large scale features can be represented. Taking into account that most of the commercial softwares only offer structural grids, it is not hard to imagine reservoir scenarios that will cause problems for the reservoir softwares, i.e. discretization of faults.

Generally, the purpose for most of the reservoir tools is to construct geological models that capture the geometry of reservoirs. Many softwares have developed good algorithms for such problems. When we involve dynamic forces in a reservoir, i.e. fluid flow, many commercial reservoir softwares fail to do this with acceptable results, especially for complex reservoirs.

Another drawback is that industrial modeling tools only allow a double continuum. Hence, it is challenging to decide which structures to include in which continuum. As mentioned earlier, many commersial reservoir softwares use stuctured grids in order to create the geological model. Since these softwares implement faults as single surfaces, they must introduce split in the

grid in order to account for juxtaposition. They try to solve this problem by introducing a transmissibility modifier to capture the flow across the faults. Unfortunately, the transmissibility modifiers largely fails to account for fluid flow along fault zones.

5.2 Structuring Fault Data for Numerical Modeling Purposes

In a reservoir, faults and fractures occur at different lengths and they also vary in thickness. This involves input data that diversify on different scales, from a centimeter-scale to a meter-scale. It is also a challenge in all fault modeling computations, to break down the physical problem to distinct scales. After the data has been seperated in scales, a geological model can be formed, see Chapter 1. This prosess involve a lot of upscaling procedures in order to form the geological model and errors can be introduced in each upscaling procedure.

In this thesis, we will model deformation bands. The fault data is given such that the deformation bands form a reservoir volume of 20m*1m*2m. In order to avoid problems because of a small volume, such as convergence problems in Eclipse, we scaled all coordinates with a factor of 100. This transformation adds some additional problems, such as a larger effect of gravity, see Appendix C.

5.3 From Faultdata to a Numerical Model

We will now describe the workflow from the input fault data to the two dimensional numerical model which will represent deformation bands and can be used for flow simulations. As we mentioned in the beginning of this chapter, we have used both Irap RMS 9.0 and Havana Robusto in order to develop the numerical model.

5.3.1 Reservoir Volume

We start the process in Irap RMS. Irap RMS is organized in different menues. A new Irap RMS-document contains certain menus with empty information in each meny. In order to construct a numerical model, we must define the top- and bottom layer by using the menu *Straigraphic framework* under the *Horizons* menu. The size of the model is restriced by points we include in Irap

RMS. These points are chosen such that we construct the correct reservoir volume.

5.3.2 Layers

When we have adapted the points, we must create layers. For Irap RMS to recognize for instant a fault created in Havana, layers must intersect the fault such that the program can get information about the fault. Therefore it is neseccary to have enough layers such so that all faults will intersect with a layer. In this thesis, we have chosen a large number since the length of deformation bands can be small. As a consequence, the distance between each layer is small and all the deformation bands constructed in Havana will be included in Irap RMS.

5.3.3 Gridding

When it comes to gridding of the model, we know that Irap RMS only offers a structured grid. We construct the grid between the top- and bottom layer, and we can choose the number of grid-blocks we want from the menu *Create Modeling Grid*. Our numerical model contains 1000 times 100 grid cells. We choose the grid to be a corner-point grid because Eclipse uses such a grid. In order to define a corner point grid, we must first define a coordinate line since the corners in a grid in Eclipse cannot be arbitary. This coordinate line is a straight non-horizontal line defined between a top coordinate and a bottom coordinate. Except for edge cells, any coordinate line is associated with four coloums of cells. The constraint defined by Eclipse is that cell corners lie on the coordinate line for all layers in the z-direction. A structured grid which satisfies the coordinate line restriction, is called a corner point grid.

5.3.4 Petrophysical Information

In order to fill the volume with petrophysical information such as porosity and permeability, we can do that in, at least, two different ways. The first possibility is via the menu *Petrophysical modeling*. The result will give statistical petrophysical data. The other method, which we have used in this thesis, is via the menu *Create new parameter* where the data is given in a continous manner. Permeability in all directions and the porosity is constructed via this menu. The permeability in all three directions are for simplicity set to 1, but we will change this value later. The porosity is defined to be 0.2 which is a reasonable choice.

5.3.5 Faults

At this point we have created a grid model for a given geometry which is filled with petrophysical information. This information is exported to Havana in order to construct faults. In Havana, faults are not just simple planes or surfaces as they are in many commercial software, see Section 5.1, but objects with properties that can act on, and modify, reservoir models. This is the reason why we construct faults in Havana and not in Irap RMS. A file containing information about the faults, such as coordinates, fault length, displacement, etc, is included in the Havana model file. The code we run is given in Appendix B, Section B.2.

5.3.6 Putting the Model Together

When the faults are constructed, we import the data from Havana back to Irap RMS. In order to include new faults, we must construct a new discrete parameter and run the script given in Appendix B, Section B.3. As a result, we have constructed a numerical model which represents the deformation bands. At the end, we must change the permeabilities. Since we want to model a fault damage zone containing deformation bands, we want the permeablity in the matrix to be higher than in the deformation bands. We set the permeability in the matrix to be 1000 mD, and the permeability in the deformation bands to be 10 mD. It should be mentioned that we choose the permeability to be the same in both coordinate directions.

5.4 Simulation in Eclipse

For reservoir simulations, we have used Eclipse in this thesis. We start the simulation 1. Jaunary 2005 and the simulation stops 1. January 2017. In Appendix B, the model file we have used for all simulations is presented. We will now give an overview over the different sections in the model file. The lecture notes by Pettersen (32) has been used as a guideline for this presentation. Result from all the simulations are given in Chapter 6.

5.4.1 The Grid

We have included the grid we constructed in Irap RMS into Eclipse. All flow-dependent parameters change continuously with time, but a simulator cannot handle continous variables. As a consequense, we must divide the reservoir into a finite number of discrete elements and define time development in a discrete sense. All properties will then be understood as being constant

within one element at a given time. A large number of grid cells will exceed the available computer memory and thus have a long runtime.

5.4.2 Petrophysics

A disadvantage with Irap RMS, is that it only allows diagonal tensors. This can cause problems for the permeability since it is a tensor variable. Most upscaling procedures result in a full tensor description, and thus there is a limited number of upscaling techniques to be used which result in a diagonal tensor. In the file we include in Eclipse, values of permeability and porosity is given in each grid block.

5.4.3 Fluid Proberties

In the model file, PVT-relations and relative permeabilties for oil and water are given in tables. We have neglected capillary pressure for both phases. In order to neglect the effect of gravity, we defined the density for both fluids to be equal. This is of course not physically correct, but Eclipse does not have any possibility to neglect the gravity, i.e. setting $g = 0$. In Appendix C, we compare a simulation with a rotated model in order to observe the effect of gravity.

5.4.4 Soil Properties

In most reservoir simulators, soil properties are simplified. In our model file we have assumed a constant compressibility.

5.4.5 Equilibration

By assuming that the fluids are in equilibrium at no-flow conditions, we only need to give the depths of the oil-water contact and the fluid pressures at a reference depth in order to calculate the initial state of the reservoir. Since we want the reservoir to be initially fully saturated with oil, the oil-water contact is defined to be higher than the height of the reservoir.

5.4.6 Well Specification

The only way for fluids to enter or disappear a reservoir in Eclipse, is through wells. We specify the positions of the wells, at which depth they are open and the production and injection rates. Since we want to compare the fine scale model with coarser models, we must place the wells in the same position

and let them be open at the same depth for all cases. In order to be able to compare all the simulations, we do not want the simulation to be controled by the bottom hole pressure. That is the reason for why the injection and production rates are so low and why we change the injection rate after one year.

5.4.7 Dynamics

Quite frequently, we must change parameters during the simulation. Such events are handled by defining dates at which operating conditions may change, see section above.

5.4.8 Output

There is a lot of information that Eclipse can calculate, and hence the amount of possibile outputs are enormous. In the model file, we have given some output-parameters in order to check and compare the result from the simulations.

Chapter 6

Upscaling of Deformation Bands

We have constructed a numerical model containing 1000 times 100 grid cells, see Chapter 5, and now we want to upscale the model in order to reduce the simulation time. In this thesis, we have used a pure local upscaling procedure. The upscaling code is written in MATLAB and developed by Dmitriy Kolyukhin. We will also present the geological model and simulation results on the fine scale and for two local upscaling procedures. We focus on the oil saturation and the field pressure for each model.

6.1 The Local Upscaling Procedure

We are studying a 2D-problem with coordinate axes x and z where x indicates the distance and z the height. They are both measured in meters. It is common in reservoir problems to let the axis which indicates height, point downwards. So is the case in our problem.

As input to the code, we must define the length of the domain in both x- and z-direction. We set $L_x = 2000$m and $L_z = 200$m. Next we state the numbers of coarse blocks in x- ($N_{c,x}$) and z-direction ($N_{c,z}$). In this thesis, we have constructed two coarse scale models - a 20 x 2 coarse model and a 40 x 4 coarse model. Each coarse block is further regridded by the MATLAB code such that each coarse block contains 80 x 80 grid cells ($N_{f,x} = N_{f,z}$) which we are using in the upscaling process. Information about the width of the deformation band (w) is then given. The width of the deformation bands is the same as the width of the grid cells in the numerical model. Hence, we find the correct width by dividing the length of the numerical model, measured in the x-direction, by the numbers of grid cells in the same

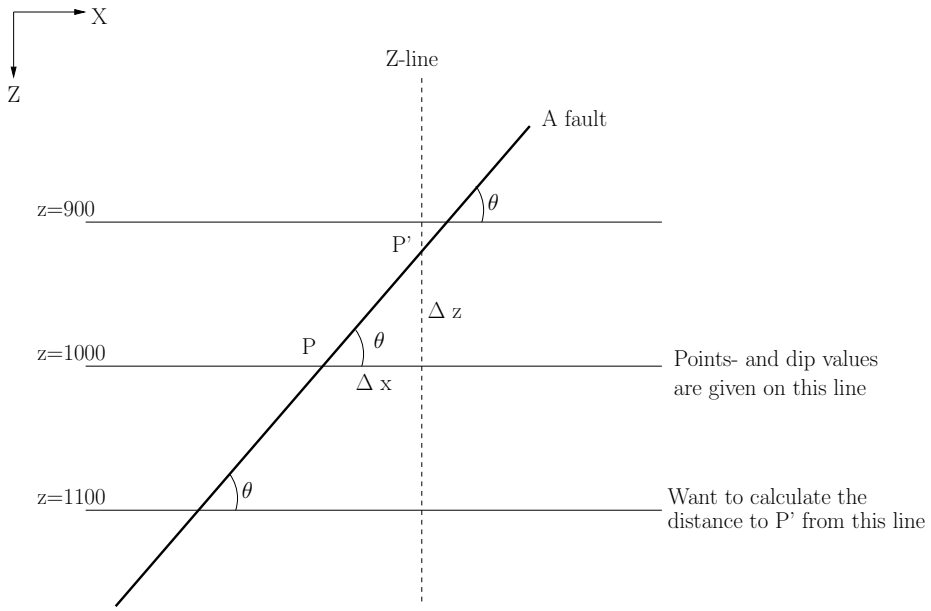

Figure 6.1: Simple trigonometry is used in order to transform points given on a horizontal line at $z = 1000$ to a horizontal line at the bottom of the model ($z = 1100$).

direction. Mathematically this is formulated as $\frac{L_x}{1000}$ which gives us $w = 2$m. Afterwards, we must assign the permeability for the matrix $K_m = 1000$mD and for the deformation bands $K_d = 10$mD. The numbers of deformation bands (N) must also be given in.

The same fault data file we used for constructing faults in Havana has point- and dip-values given on a horizontal line at the depth $z = 1000$m, see Figure 6.1. In order to calculate correct upscaled permeability tensors K^* with the program, we must calculate the intersection of the faults with a vertical line. This line, called Z-line in Figure 6.1, must be placed in the middle of the numerical model, measured in the x-direction ($\frac{L_x}{2}$). Simple trigonometry is used for the calculation of intersection points. Let P be the point we know on the horizontal line at $z = 1000$m and add 100m in order to transform the values to the bottom line ($z = 1100$m). Then we have the following relation between the points with reference to Figure 6.1,

$$P' = \Delta z + 100\text{m} = \tan\theta * \Delta x + 100\text{m} \quad . \tag{6.1}$$

All these intersection points must be given as a vector in the code. The final input we must give the code, is a vector containing the angles of each

deformation band.

The code calculates the upscaled permeabilty tensor by the procedure given in Section 3.1.5. A program which calculates a full tensor is also developed. It follows the desription given in Section 3.1.6. By using a diagonal tensor instead of a full tensor in domains where the density of faults is high, we introduce errors in our upscaling process, see Section 6.7.

6.2 The Geological Model

This thesis focus mainly on upscaling of a geological model containing deformation bands, see Figure 6.2. The permeability in the deformation bands is set to be 10 mD and in the matrix the permeability is 1000 mD. We are running a quarter of five-spot simulation on the fine and upscaled models. The injection well is placed in the corner, down to the right, and the production well is placed in the opposite corner, up to the left. As we can see in Figure 6.2, the number of faults increase as we move from right to left. Hence, it is expected that the water front will move slower as the simulation time goes by. In some domains, we can see that the deformation bands form a channelized system. In addition, we can see that many deformation bands intersect with eachother.

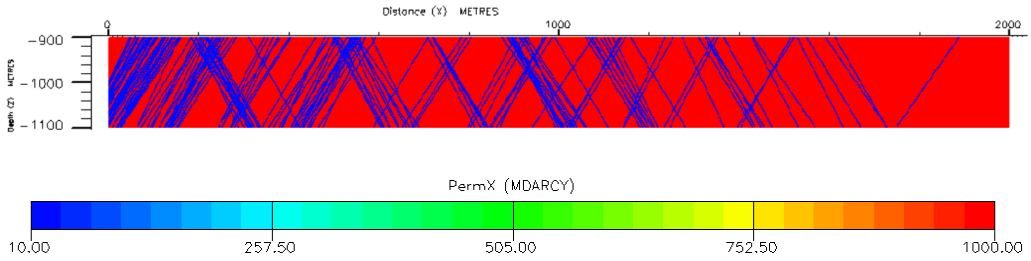

Figure 6.2: The geological model showing the distribution of deformation bands. The x-axis gives the distance while the z-axis indicates the depth, both are measured in meters. The permeability in the matrix is set to be 1000 mD and for the deformation bands, we have used a permeability value of 10 mD.

6.3 Fine Scale Simulation

The results from the fine scale simulation, are treated as the true solution. Although this simulation do not have any problems or errors, there are some

information we should be aware of. The discretization of faults depends on the grid size, see in Section B.3 in Appendix B. This means that if we increase or decrease the number of grid cells in the fine scale model, the width of the faults will be changed.

Figure 6.3 shows the saturation distribution at some given times. We can see that the water front after one year has moved longer relatively to the results after two years at other dates. This can be explained by the increasing number of faults as the water front moves forward. Further, we can see that the water front moves relatively steep expect from the first figure and the last figure. At those dates, the water front is in an area with a low number of deformation bands and there are no deformation bands intersecting eachother. Since the permeability in the deformation bands are much lower than the case is for the matrix, the water front will move the way with lowest resistance and hence the front will be less steeper. At the other dates, we can observe from the geological model, Figure 6.2, that there are deformation bands crossing eachother and as a result cause the steep water front.

6.4 Step 1 - Coarse Gridsize of 20 x 2

Before we started simulations on this scale, we knew that a local upscaling procedure that transfer a fine scale model with 1000 times 100 grid cells to a coarse scale model with 20 times 2 grid cells would not represent the fluid flow well. But such a coarse upscaling procedure can be used in the first step in the algorithm we presented in Chapter 7 in order to get estimated pressure values. The upscaled permabilities values in each block is given in Figure 6.4. We can see that the upscaled permeability values decrease from right to left. This was expected, since the number of deformation bands increase from right to left. The result from the simulation run on this scale is given in Figure 6.5. We observe that the saturation front is moving faster than it does in the fine scale simulation.

6.5 Step 2 - Coarse Gridsize of 40 x 4

We have used the same upscaling procedure as we did in the section above, but now with a coarse model containing 40 times 4 grid blocks. Figure 6.5 shows the upscaled permebility distribution and we can observe the single fault to the right in the geological model. We can also observe more blocks with higher permeability to the left in the model than the case is for the step

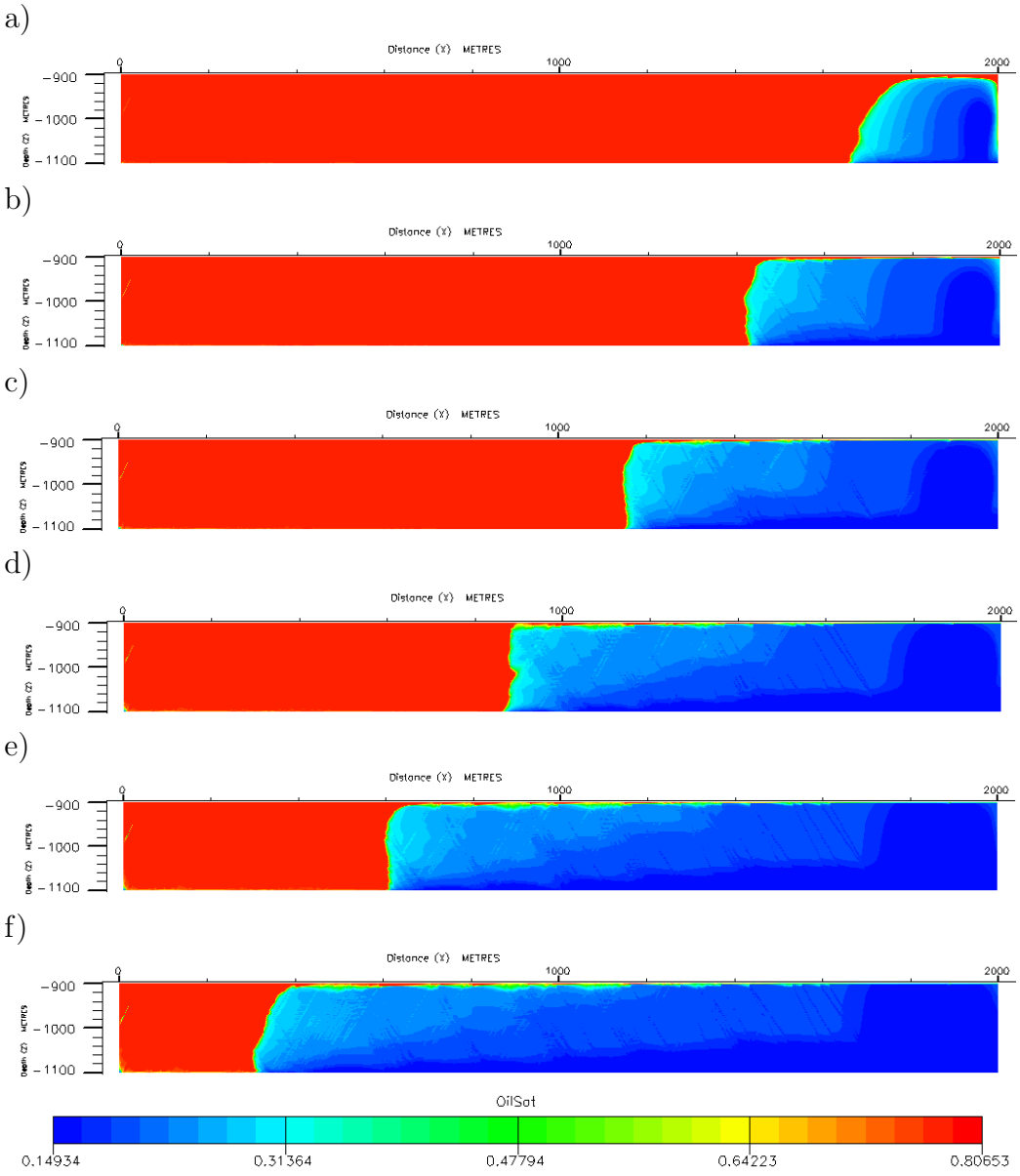

Figure 6.3: Simulation results after a) 1. January 2006 b) 1. January 2008 c) 1. January 2010 d) 1. January 2012 e) 1. Janurary 2014 and f) 1. January 2016. The x-axis gives the distance while the z-axis indicates the depth, both are measured in meters.

a)

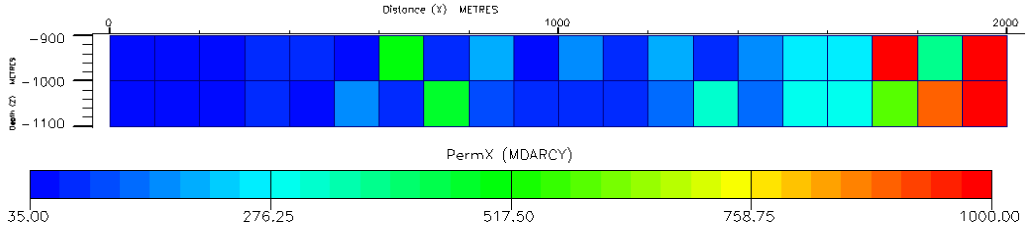

b)

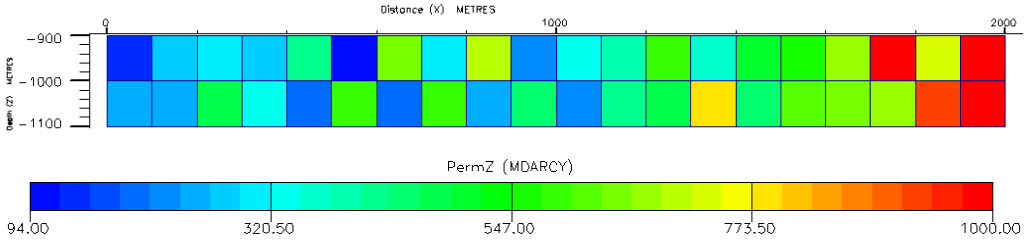

Figure 6.4: Upscaled permeabiltiy in mD for step 1 in a) x-direction b) z-direction. The x-axis gives the distance while the z-axis indicates the depth, both are measured in meters.

1 permeability distribution. Hence, we can see that the faults are distributed as a system of channels in some regions. Figure 6.7 shows the simulation at the same dates as in the global fine simulation and the step 1 simulation. If we compare the simulation results with the fine scale and the step 1 simulation, we can see that the front is moving faster than the fine scale simulation but slower than the step 1 simulation.

6.6 Pressure Comparison

We will in this section present field pressure curves for all the simulations. We can see in Figure 6.6 that although we increase the number of coarse blocks in the upscaling procedure, we do not get closer to the fine scale pressure curve. This demonstrate the weak side of pure local upscaling procedures as we will discuss in Section 6.8. The difference in pressure increases as the simulation time goes by. As we can see in the model file we use in Eclipse, see Section B.4 in Appendix B, we change the injection and production rates after one year (1. January 2006) because we want the wells to be controled by the rates in order to compare the different pressure curves for the different flow scenarios. This is the reason for why we have the buckling point at this date. If the injection and/or production rates are choosen too high in Eclipse,

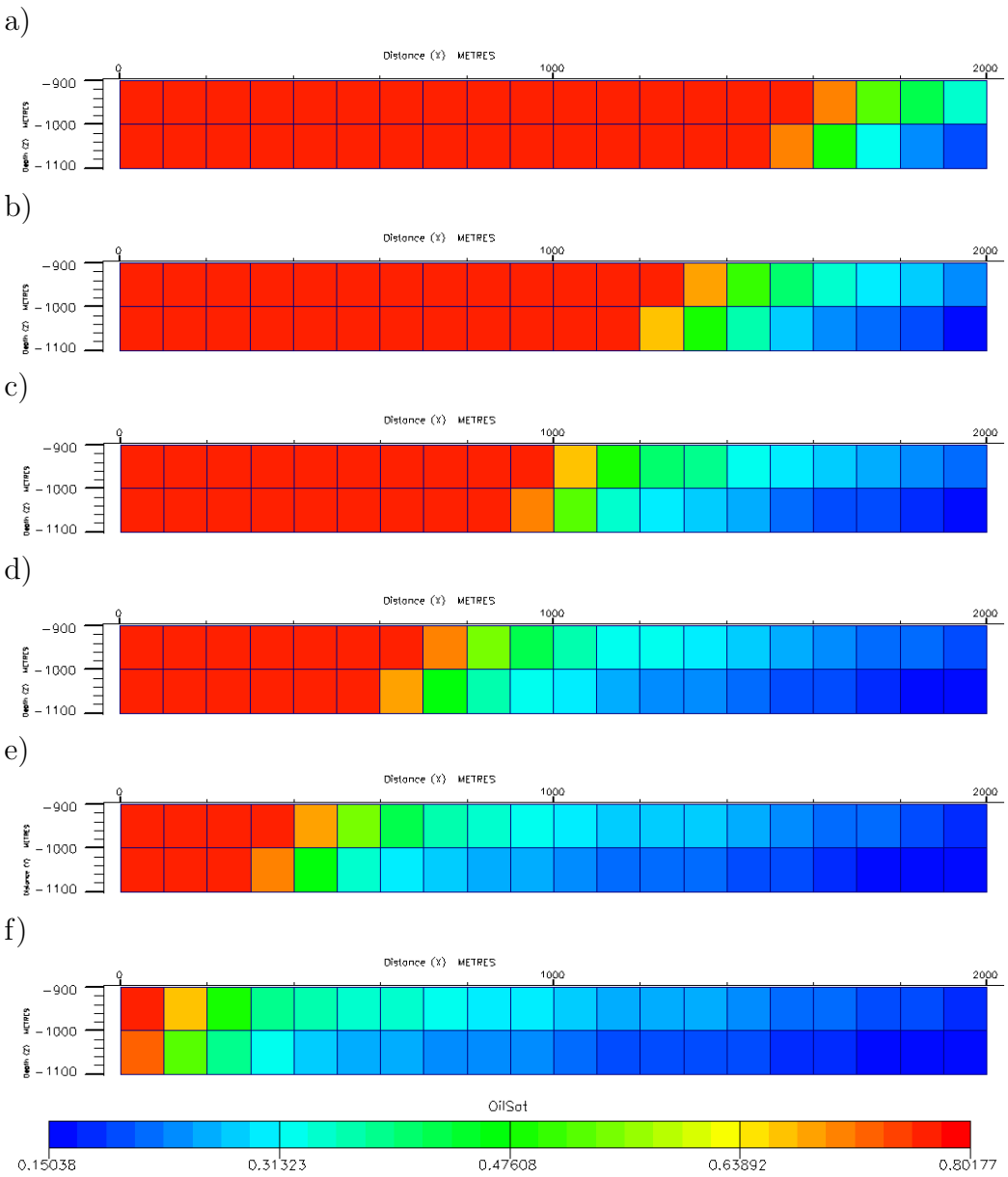

Figure 6.5: Simulation results after a) 1. January 2006 b) 1. January 2008 c) 1. January 2010 d) 1. January 2012 e) 1. Janurary 2014 and f) 1. January 2016. The x-axis gives the distance while the z-axis indicates the depth, both are measured in meters.

a)

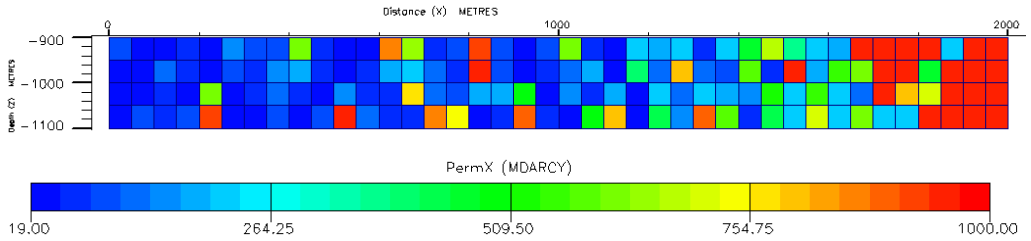

b)

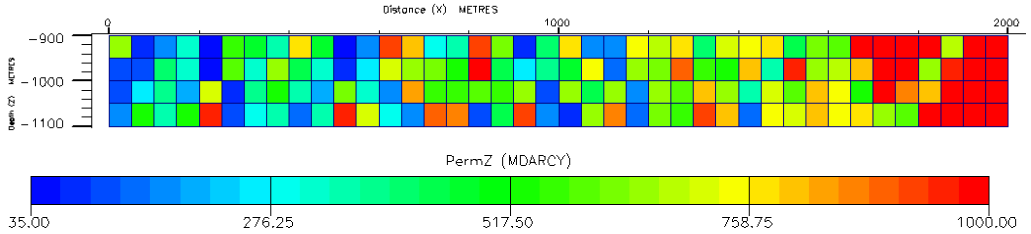

Figure 6.6: Upscaled permeabiltiy in mD for step 2 in a) x-direction b) z-direction. The x-axis gives the distance while the z-axis indicates the depth, both are measured in meters.

very often the wells will be controled by the bottom hole pressure. This is not profitably because the injection and production rates are then no longer constant and the same for all simulations. It results in pressure curves that we can not use to compare other simulations since the conditions are not the same for all simulation runs.

6.7 Comparison of Full- and Diagonal Tensors

In this section we will compare full and diagonal tensors for some selected domains. It is likely to believe that where the numbers of deformation bands increase, we should use a full tensor. Unfortunately, the available software programs we have used in this thesis only allow diagonal tensors to be incorporated. The comparison is done for the first upscaling step, going from 1000 times 100 grid blocks to 20 times 2 grid blocks. With the boundary conditions we have used for the full tensor permeability calculation, the tensor will be symmetric, $K^*_{i,j} = K^*_{j,i}$, and positive definite, i.e. have positive eigenvalues.

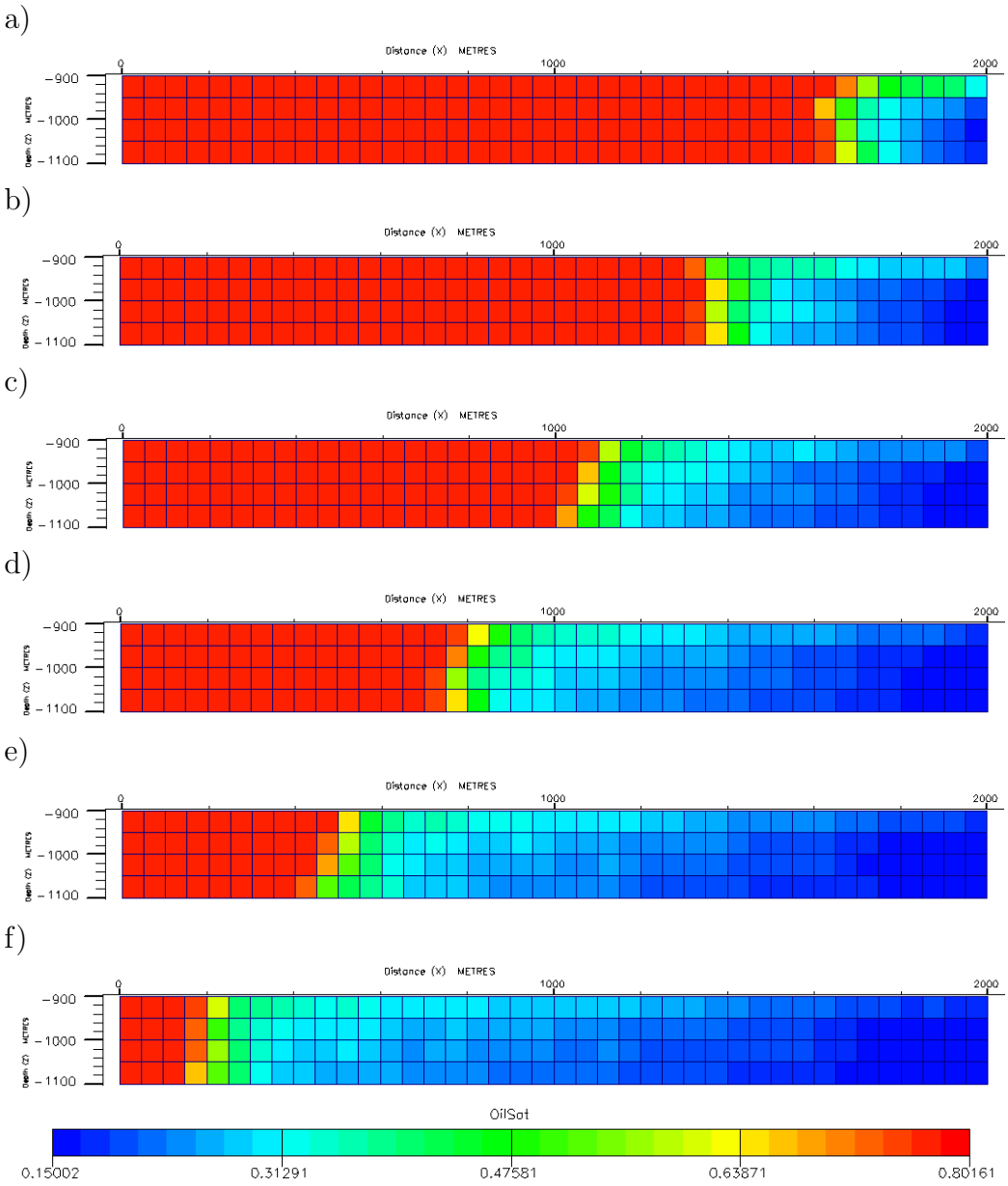

Figure 6.7: Simulation results after a) 1. January 2006 b) 1. January 2008 c) 1. January 2010 d) 1. January 2012 e) 1. Janurary 2014 and f) 1. January 2016. The x-axis gives the distance while the z-axis indicates the depth, both are measured in meters.

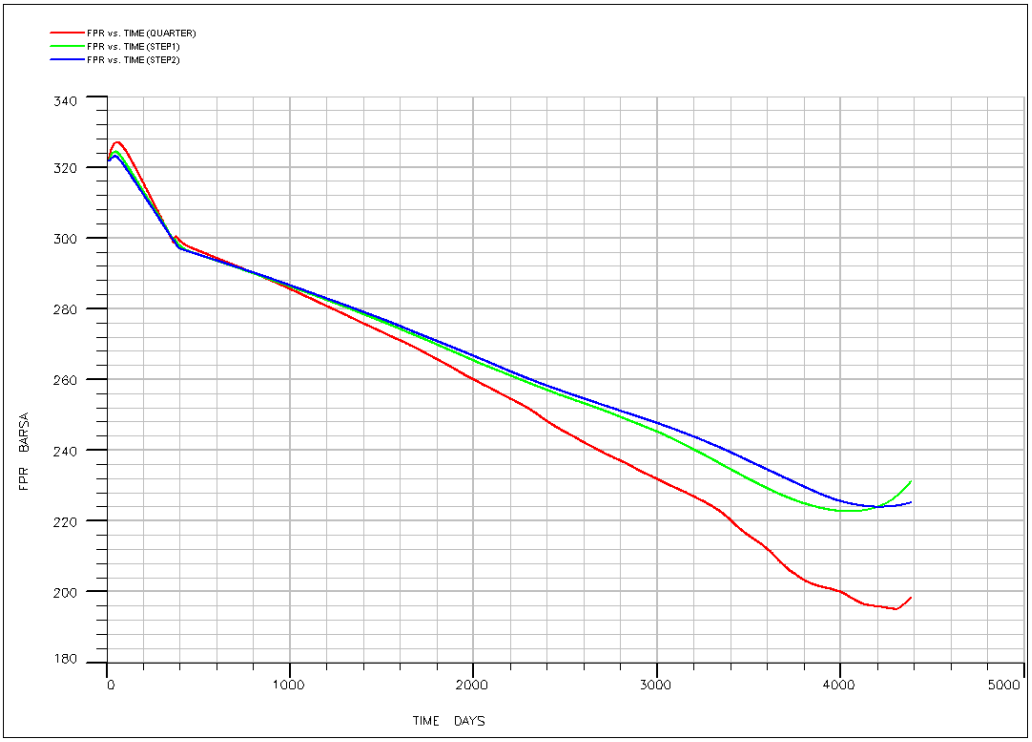

Figure 6.8: A comparison of field pressure for all simulations. The red line represents the fine scale field pressure, the green line the field pressure in the step 1 attempt and the blue line shows the field pressure after step 2. The x-axis shows the time in days while the pressure is given on the y-axis.

6.7.1 Domains

We begin by presenting the domains we are studying, see Figure 6.9. (a) and (b) represent domains with a large number of deformation bands. (c) is an example of a domain where it is expected that the result from a diagonal- and full tensor calculation is close i.e. the off-diagonal elements are small in the full permeability tensor.

6.7.2 Full- and Diagonal Tensor Results

In this section we will state the results from diagonal- and full permeability tensor calculation for the domains shown in Figure 6.9. Observe that for domain (a) and (b) we get negative values for $K^*_{1,2}$ and $K^*_{2,1}$ in the full permeability tensor calculation. As long as the permeability tensor is symmetric and positive definite, we can accept those values by Onsager's principle. Since element values in tensors depend on how we construct the coordinate system, negative element values may occur. When we compare K^*_{full} with K^*_{diag} in domains (a) and (b), we can see a significant difference in each element. We are therefore loosing information when we restrict ourselves to just use diagonal tensors. For domain (c), the size of the off-diagonal elements are small in the full tensor calculation and thus the use of a diagonal tensor can be justified.

- Domain (a)

$$K^*_{full} = \begin{bmatrix} 190 & -202 \\ -202 & 400 \end{bmatrix} \text{mD} \tag{6.2a}$$

$$K^*_{diag} = \begin{bmatrix} 66 & 0 \\ 0 & 281 \end{bmatrix} \text{mD} \tag{6.2b}$$

- Domain (b)

$$K^*_{full} = \begin{bmatrix} 148 & -139 \\ -139 & 299 \end{bmatrix} \text{mD} \tag{6.3a}$$

$$K^*_{diag} = \begin{bmatrix} 50 & 0 \\ 0 & 242 \end{bmatrix} \text{mD} \tag{6.3b}$$

- Domain (c)

$$K^*_{full} = \begin{bmatrix} 151 & 19 \\ 19 & 403 \end{bmatrix} \text{mD} \tag{6.4a}$$

$$K^*_{diag} = \begin{bmatrix} 82 & 0 \\ 0 & 302 \end{bmatrix} \text{mD} \tag{6.4b}$$

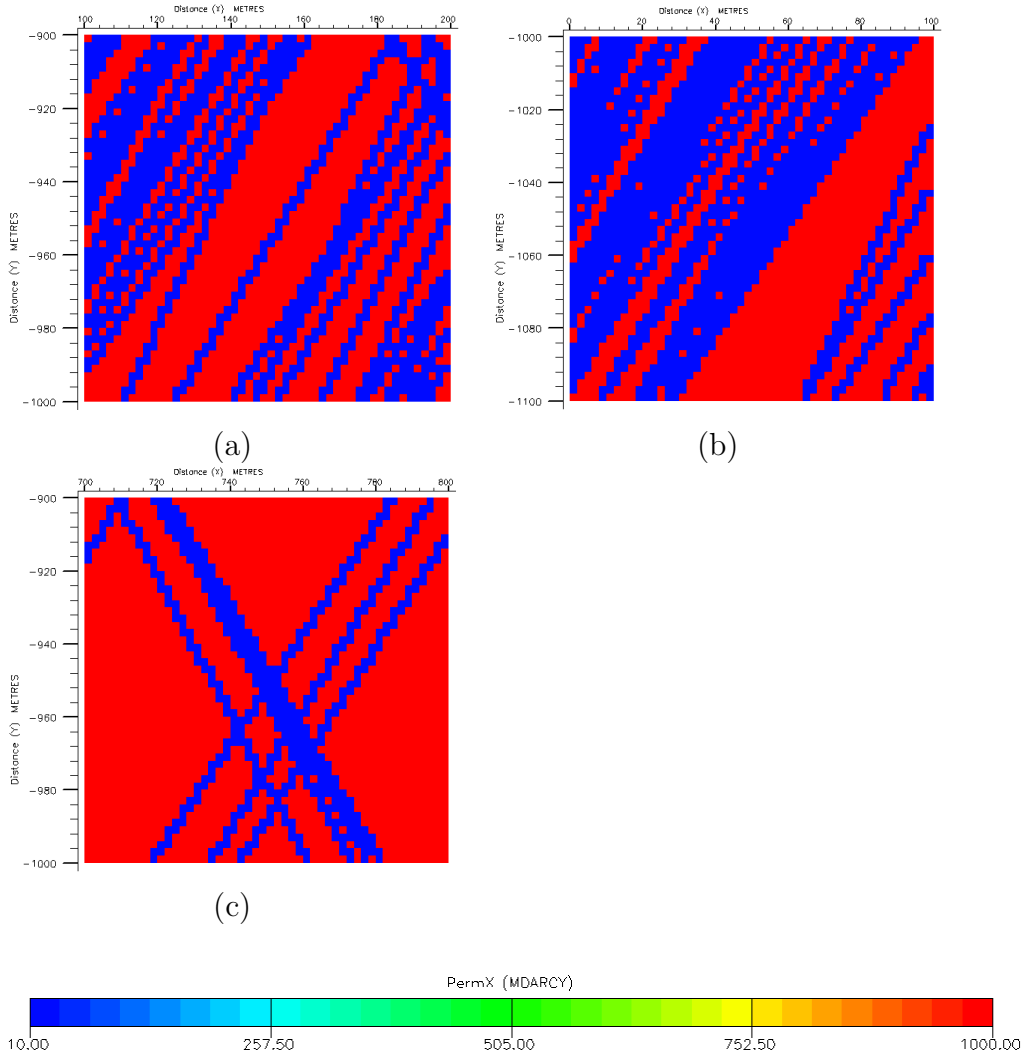

Figure 6.9: Domain (a), (b) and (c) for calculation of diagonal- and full permeability tensor. These domains are subdomains of the geological model. The x-axis gives the distance while the z-axis indicates the depth, both are measured in meters.

6.8 Discussion

The use of a pure local upscaling technique is a matter of debate. The dependecy on the imposed boundary conditions for such methods is not profitable, see i.e. Wen et al. (40). In the code we have used, fixed boundary conditions with a linear pressure variation along the sides parallel to the direction of the pressure gradient are used. We can see from Figure 6.6 that the coarse scale pressure curves do not match the fine scale pressure curve with a satisfactory result. The pressure curve for step 2 (40 x 4 grid cells) is almost the same as the case is for the step 1 (20 x 2 grid cells) pressure curve. We believe that by using the pressure values in each coarse block from the 20 x 2 grid simulation in an extended upscaling procedure to a 40 x 4 gridmodel, we would have achieved a better approximation to the fine scale pressure solution. Such an attempt would have given us a full upscaled permeability tensor which we unfortunately can't handle with the available programs we have used in this thesis. Overall we can conclude with that the local upscaling procedures do not fit the fine scale pressure curve well, but we can see in Figure 6.6 that the upscaled pressure curves fit the fine scale pressure curve very good in the start of the simulions (until around 1000 days). In this period, the water front is in a domain with few deformation bands and local upscaling procedures work well. After this period, the number of deformation bands increase and the local upscaling technique fail to represent the fine scale pressure curve with an acceptable result.

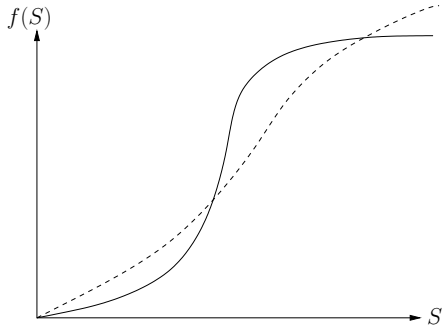

Figure 6.10: An simplified illustration of a fine (the full line)- and a coarse (the dotted line) scale fractional function.

We suggest in our new algorithms in Chapter 7 to use an extended upscaling procedure in order to reduce the effect of boundary conditions. By using a border region when we want to upscale the permeability K, we will be able to capture more effects of the large scale conductivity of the perme-

ability field. As a result, we should provide a more accurate K^* than we will do by using a purely local approach.

The simulation results from the upscaled models do not give an acceptable description of the fluid flow. The main reason is that we have used too few target coarse blocks. When we do such a coarse upscaling procedure, the S-shaped flux function will be spread out compared to a flux function for a fine scale, see Figure 6.10. It results in a water front moving faster and it becomes less steep than the case is for a fine scale simulation, see Figures 6.3, 6.5 and 6.7. As a consequence, the fine scale simulation water front has not come as far as the case is for the step 1 simulation in 1. January 2016. We can even see the difference when we compare the two upscaled models.

Chapter 7

Hierarchy Upscaling Algorithms

In this chapter, we will present two hierarchy upscaling algorithms which should be applied on a two dimensional representation of a fault damage zone with coordinate axes x and y. Unfortunately, the available numerical softwares we have used in this thesis can not handle the algorithms because of problems handling tensor-variables.

7.1 A Hierarchy System of Scales

A damage zone represents faults with different lengths and thickness, see Figure 7.1 for a simplified illustration. In our algorithms, we will use this fact by seperating the faults in different scales. This hierarchy division is done in order to include the effect of all faults. We will base our algorithms on an adaptive local-global upscaling procedure which is presented in Chen and Durlofsky (8). We start on the finest scale, and we want this scale to capture the faults which are short and thin, i.e. deformation bands.

7.2 An Uniform Upscaling Procedure

The first algorithm we present begins by constructing a global uniform grid. In each block, an upscaling procedure will then be applied as we will describe in the sections below and an iteration process starts. A summary of the algorithm is given at the end of the section.

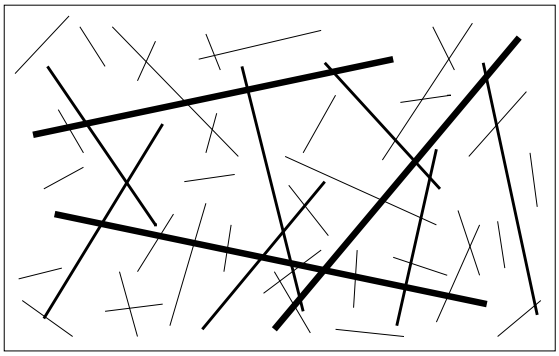

Figure 7.1: An example of a simplified fault damage zone which is modified for numerical purposes. The smallest faults typically represent deformation bands.

7.2.1 Upscaling from a Geomodel to a Global Coarse Scale

Most upscaling procedures which are based on a local-global coupling, must run a global fine scale simulation in order to get boundary condition for the local upscaling procedures. In order to avoid a global fine scale simulation, we first upscale the entire model to a global coarse scale by using a pure local upscaling technique. This process will give us upscaled permeability tensors for each coarse block. By running a new simulation on the global coarse scale, we can find pressures values in each coarse block which we will use as boundary conditions in an extended local upscaling procedure. Averaged pressure gradients ($\overline{\nabla p}$) are calculated by Equation (3.38). Fluxes can be found by the following equation

$$q^* = -K^* \frac{\overline{\nabla p}}{L_1} L_2 \quad , \tag{7.1}$$

where we use the upscaled permeability tensor K^* from the local procedure, L_1 is the length of the target coarse block in x-direction and L_2 is the length of the target coarse block in y-direction.

7.2.2 The Coupling Between the Coarse Scale Global Flow and the Coarse Scale Blocks

The global coarse scale model we constructed in the section above, will in many cases not give a simulation with acceptable result compared to the fine scale simulation. We will therefore apply an extended local upscaling

technique with $d = 0.5$ on the same target coarse blocks. Here d indicates the distance from the target cell to the ring where the boundary conditions are computed, measured by the size of the target cell. In order to get boundary conditions between the coarse block pressure values, see Figure 7.2, we will use an interpolation formulation. For new pressure values in the x-direction, we apply the following formula

$$p_{i,x} = p_1^* + (x_i - x_1)\frac{p_2^* - p_1^*}{x_2^* - x_1^*} \qquad \text{where} \quad x_1^* < x_i < x_2^* \quad . \tag{7.2}$$

With reference to Figure 7.2, p_1 indicates the first coarse block pressure value in the interval we want to find interpolated pressure values in and p_2 is the next coarse block pressure value. We define x_1 and x_2 in the same manner, but they indicate distance. x_i is a point between x_1 and x_2. For the y-direction, the interpolation formula becomes

$$p_{i,y} = p_1^* + (y_i - y_1)\frac{p_2^* - p_1^*}{y_2^* - y_1^*} \qquad \text{where} \quad y_1^* < y_i < y_2^* \quad . \tag{7.3}$$

All magnitudes are defined before, but with a modification to the y-direction.

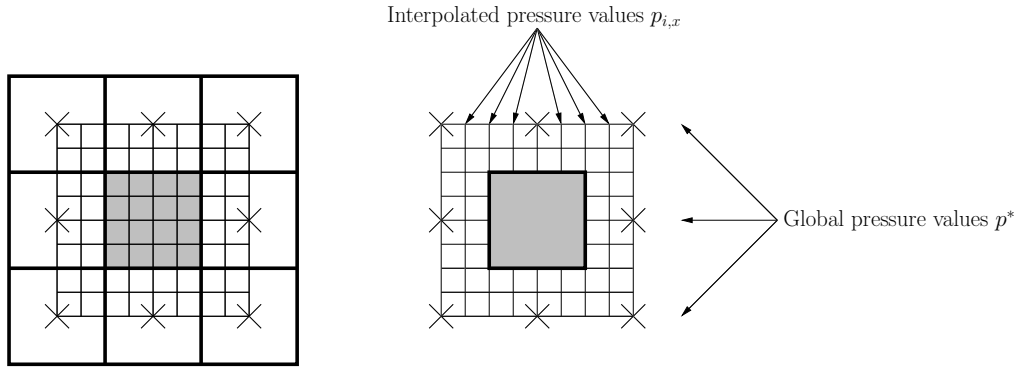

Figure 7.2: An illustration that shows the interpolated pressures values and the pressure values found from the global coarse grid. The target fine cell is in grey, and we will apply an extended upscaling procedure with $d = 0.5$.

The boundary conditions we need in order to solve the extended local upscaling problem are now calculated, and we can find the upscaled permeability tensor K^*.

7.2.3 Calculation of K^*

By using an extended local upscaling procedure, we achieve a full permeability tensor for each target coarse block. We follow the decription given in Section 3.1.6 in Chapter 3, but with the new pressure boundary conditions we have found in the section above. We use the averaged pressure gradient from the last simulation, but we need to solve Equations (3.37), (3.43) and (3.44). Afterwards, we move on to the next coarse block and follow the same description.

7.2.4 A Global Comparison of the Pressure

After we have found new permeabilities, we run a new simulation in order to get new coarse pressure values in each coarse block. We need a criteria so that we know whether we shall continue or stop the iteration process. We check this by calculating a L_2 norm defined as

$$\|\delta p^*\|_2 = \left[\frac{1}{N_{c,x}N_{c,y}}\sum_{i=1}^{N_{c,x}}\sum_{j=1}^{N_{c,y}}((p^*_{i,j})^\tau - p^*_{i,j})^{\tau-1})^2\right]^{1/2} < \epsilon \quad , \qquad (7.4)$$

where $\tau = 1, 2, 3, ...$ is the iteration number and ϵ is the limit of convergence. If the convergence test fails, we must use a finer grid in the upscaling procedure and repeat the steps above. Otherwise, the matrix will now be the upscaled permeability in the next scale. We continue with the process described above, but introduce larger faults.

We must be aware of that the new simulation may not represent the fluid flow well although we have regridded the blocks and iterated until acceptable pressure values have been found. We may have choosen a too coarse grid in the upscaling procedure from the geological model to the global coarse model.

7.2.5 The Uniform Upscaling Algorithm

1. Perform a local upscaling procedure. In general, we suggest a coarse model which contains 10 prosent of the fine scale grid cells.

2. Run a simulation in order to get initial pressure values in each blocks.

3. Regrid the model. Increase the number of grid cells to the double i.e. 20 x 2 becomes 40 x 4.

4. Calculate the interpolated pressure values by Equations (7.2) and (7.3).

5. Upscale the model by an extended local upscaling technique.

6. Run a new simulation with new permeabilities.

7. Compare pressure values from iteration τ and $\tau - 1$ by checking the convergence of simulation in point number 2 with simulation in point number 6. We use Equation (7.4) for this purpose.

8. If the convergence test fails, do 3 - 7 again with pressure values from the last iteration.

9. Else, move to the next scale in the hierarchy system and introduce new faults.

7.3 An Adaptive Upscaling Procedure

We will also present an adaptiv upscaling algorithm which doesn't construct a global uniform grid. It differs from the uniform algorithm in the way that we also check the convergense of permeability in each block before we move to the next block in the grid. We also check the convergence of pressure on the global scale.

7.3.1 Check of Convergence in Each Block

After we have found a new permeability value in a block, we introduce a criteria in order to know if we must use an even finer grid on the target coarse block to achieve a better value. We do this by calculating the norm defined as

$$\|\delta K^*\| = \left[((\|K^*_{i,j}\|_f)^\tau - (\|K^*_{i,j}\|_f)^{\tau-1})^2\right]^{1/2} < \epsilon \quad , \tag{7.5}$$

where τ is the iteration step, ϵ is the limit of convergence and $\|\cdot\|_f$ is the Frobenius norm defined for a $M \times N$ tensor K with elements $k_{m,n}$ as

$$\|K\| = \left(\sum_{m=1}^{M}\sum_{n=1}^{N}(k_{m,n})^2\right)^{1/2} \quad . \tag{7.6}$$

The iteration process on each target coarse block will continue until we have found an acceptable value for the changes in the permeability δK^*.

7.3.2 The Adaptive Upscaling Algorithm

1. Perform a local upscaling procedure. In general, we suggest a coarse model which contains 10 prosent of the fine scale grid cells.

2. Run a simulation in order to get initial pressure values in each blocks.
3. Grid the model adaptively.
   (a) Select block (i,j).
   (b) Regrid the block by doubling the number of grid cells.
   (c) Calculate the interpolated pressure values by Equations (7.2) and (7.3).
   (d) Upscale the block by using an extended local upscaling technique. We find a new permeability $K^*_{i,j}$.
   (e) Check convergence of the new permeability by Equation (7.5). .
   (f) If the convergence test fails, regrid it once more and do 3b- 3e.
   (g) Else, move to the next coarse block and do 3b- 3f.
4. Run a new simulation with new permeabilities.
5. Compare pressure values from iteration τ and $\tau - 1$ by checking the convergence of simulation in point number 2 with simulation in point number 4. We use Equation (7.4) for this purpose.
6. If the convergence test fails, the local upscaling procedure in point number 1 is too coarse. Do 1 - 5 again.
7. Else, move to the next scale in the hierarchy system and introduce new faults.

7.4 Discussion

The uniform upscaling algorithm is easier to implement than the adaptive upscaling algorithm. We believe that the uniform upscaling approach will have problems when it comes to upscaling of a highly heterogenous media. With such a media, the method will use a long time to finished and there may be a lot of unnecessary upscaling procedures on blocks which already have a good estimate for the permeability.

The adaptive upscaling algorithm has its advantegous that it will discover regions where the permeability difference between a iteration step is low. As a result, we avoid unnecessary regridding and new upscaling procedures on blocks we already have found a good estimate for the permeability.

Although we have found good estimates for the permeability in each target coarse block, we are not guaranteed that the global pressure convergence

test, Equation 7.4, will succeed. By constructing a finer grid in the global model, we must start the iteration process all over again. As a consequence, we must calculate new upscaled permeability tensors without using information from process before which is not beneficial.

A comparision of the two algorithms would have been interesting. In addition to compare the simulation results, a comparision of the computational time should also have been done for various heterogenous media.

We are using pressure values as boundary conditions derived from a global coarse simulation. During a simulation, the pressure changes in each block. Thus, we have the possibility to choose other pressure values than the initial ones. It would have been interesting to compare two upscaling procedures where the imposed boundary conditions in one case are the initial pressure values while we in the other case use pressure values after i.e. 3 months of production. Perhaps, the best upscaling routine would be if we had used the initial pressure values and after i.e. 3 months of production we had performed a new upscaling procedure with these pressure values. We could have continued this iteration by for example performing a new upscaling procedure every third month of production with the related pressure values. A comparison of the result from such a upscaling procedure with a upscaling process where we have only used initial pressure values should have been done.

Chapter 8

Conclusions and Further Work

In this thesis, we have built a numerical model which attempts to represents deformation bands in a fault damage zone. We have simulated on a fine and two upscaled versions of the model. In this final chapter we will summarize the results we have achieved and draw some conclusions. We will also point out some direction for further work.

8.1 Summary and Conclusions

As mentioned in Chapter 5, we had to scale all coordinates and deformation bands with a factor 100 in order to avoid convergence problems in Eclipse. It is unrealistic that we are studying deformation bands distributed over 2000 meters in the horizontal direction and with a height of 200 meters. With the discretization technique we have used, see Appendix B, it results in a deformation band thickness of 2m. Dividing this number with the scaling factor, we are on the centimeter scale. With reference to Chapter 4, the width of deformation bands are in the range of a few millimeters. Hence, the width of our deformation bands are not physically correct when we divide the model with the scaling factor. The discretization of faults is therefore a critical factor in this thesis. We will now illustrate the different permeability values we get in one grid block by assuming a vertical fault is intersecting a grid cell in its center, see Figure 8.1. We let the deformation band has a thickness of 0.001m with a permeability value 10 mD. The matrix has permeability 1000mD, and the grid block has the same width as we have used in this thesis after we have divided with the scaling factor. With the geometry presented in Figure 8.1, we can use harmonic averaging. The harmonic average equation, see Equation (3.10), becomes

$$\frac{1}{K_H} = \frac{1}{0.02\text{m}}[\frac{0.0095\text{m}}{1000\text{mD}} + \frac{0.001\text{m}}{10\text{mD}} + \frac{0.0095\text{m}}{1000\text{mD}}] \quad , \tag{8.1}$$

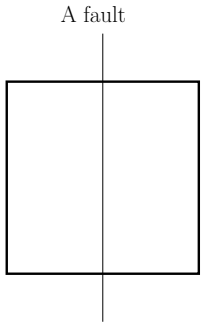

Figure 8.1: A vertical fault with thickness 0.001m intersects a grid block with size 0.02m times 0.02m.

and we get $K_H \approx 168\text{mD}$. By using the discretization technique given in Appendix B, the same grid block would have recieved a permeability value equal to the permeability value of the fault. That is 10mD. The only way we can correct the width of faults is by using a finer grid. The discretization dependency on the gridsize is not beneficial. The number of fine cells should not be defined in order to get a correct width of the deformation bands, but rather in such a way that we are able to capture the complexity of a reservoir. We recommend to use a discretization technique which can handle a distribution of various faults i.e. faults with different lengths and thickness. By using a flexible meshing algorithm resulting in triangle grid cells, we achieve a grid which can handle complex reservoirs, see i.e. Holm et al. (27).

We have focused on upscaling the absolute permeability in this thesis. The pressure equation contains a mobility factor, see Equation (2.12), which is defined to be the relative permeability over the viscosity. The relative permability depends on the saturation, and the saturation depends on the position and time. As an additional effect by including upscaling of relative permeability, we get a time-dependent upscaling procedure. A solution strategy would be to solve for the pressure and velocity by using the saturation at the present time, and advance the saturation to the next time level by using the saturation equation for two-phase flow, Equation (2.13). By including the relative permeability in the calculations, the upscaling procedure becomes more challenging because to solve Equation (2.13) numerically is not easy. From an upscaling point of view, we can solve the saturation equation by using an averaged equation strategy as it is descriped in Chapter

3. Including upscaling of relative permeability will however result in a better coarse model for describing two-phase flow.

By neglecting the capillary pressure, the saturation equation for two-phase flow becomes

$$\rho\frac{\partial S}{\partial t} + \nabla \cdot (\mathbf{u}f(S)) = 0 \quad . \tag{8.2}$$

If we further assume that the phases are incompressible with no sources and neglects the gravity, we obtain the pressure equation

$$\nabla \cdot (K\lambda(S) \cdot \nabla p) = 0 \quad . \tag{8.3}$$

For a unit mobility ratio, we have the following saturation and pressure equations,

$$\rho\frac{\partial S}{\partial t} + \nabla \cdot (\mathbf{u}S) = 0 \quad , \tag{8.4}$$

$$\nabla \cdot (K \cdot \nabla p) = 0 \quad . \tag{8.5}$$

Comparing these equations, we can see a close simularity between the unit mobility equations and the two-phase equations. This explains why permeability upscaling procedures which are developed for a unit mobility scenario, also can be used as a basis for two-phase upscaling as we have done in this thesis.

The permeability within a deformation band vary, so also the lengths. We have used the same permeability (10 mD) for every deformation band and not included a variation in permeability within the deformation bands themselves. In addition, geologists have observed that deformation bands are not connected in one line. It is common to see holes in the deformation bands. All these factors should have been incorporated in the numerical model in order to discuss the effect of deformation bands in a fault damage zone.

As mentioned earlier, deformation bands are distributed such that they in some domains form a channelized system. Wen and Durlofsky (39) have compared different channelized systems due to what kind of gridding type they have implemented. They demonstrate that by using a flow-based grid, they improve the upscaling results considerably compared to a upscaling method where they have used a uniformed grid. A flow-based grid should have been adapted in our model in order to compare the results with a uniform grid as we have used.

Eclipse does not offer the possibility to turn off the effect of gravity. Since we have scaled our model, resulting in a height difference of 200m instead of

2m, we want to neglect the effect of gravity. Therefore we have set the density for both oil and water to be equal. The range for the crude oil density in North Sea reservoirs is typically between 745-1002 kg/m^3. The water density is approximately 1000 kg/m^3. In our Eclipse model file, see Section B.4 in Appendix B, we have set both the oil- and water density to be 241.5 kg/m^3. An object with low density means that it has a large volume for a given amout of mass of the object. Hence the amount of oil and water is less than if we have used the correct density for the fluids. It is not physical correct to set them equal, but we achieve the desired effect, see Appendix C.

In this thesis, the fine scale simulation time is 2 hours and 12 minutes while for both upscaled models the simulations were finished after 9 seconds. There is a significant difference in the computational time for the simulations, but the effect of the coarse scale simulations time are reduced as they do not represent the fine scale simulation with an acceptable result. We must also take into account that running the MATLAB-program in order to calculate the upscaled permeability tensors also takes time. Thus, the actual time difference is not that large. We have datas on a 100 times 10 coarse model as well, a model which is 10 prosent of the fine scale model, but we have not yet found a suitable way to implement the upscaled permeability values into Irap RMS. We have incorporated them manually, but it should be possible to construct a method which can fix this problem.

8.2 Further Work

A crucial assumption in all of the local and extended local procedures is that the flow is described locally as linear. This means that the pressure gradient ∇p is assumed to be constant over the target coarse block region. In near-well regions, this assumption doesn't hold as the pressure of a well away from boundaries varies as $\log d$, where d is the radial distance. Near-well upscaling methods should therefore be applied in our upscaling procedure and in the algorithms we have presented in Chapter 6.

In all our simulations, we have neglected the capillary pressure. The saturation equation for two-phase flow, see Equation (2.13), contains a diffusion part $D(S, x)$ which include the capillary pressure, see Equation (2.15). By neglecting the capillary pressure, we will not describe the effect of diffusion in our simulations and the saturation equation becomes a hyperbolic partial differential equation. Capillary pressure should be included in further works in orders to get more reliable simulation results.

In further works, a method which can handle a large fault damage zone should be developed. A suggestion is to divide the model into blocks and

use domain decomposition methods on each block. It is advantageous to seperate the reservoir in such a matter, since the possibility to run upscaling procedures on the different blocks by using parallel computing is profitable. Researchers develop better and better upscaling techniques for complex reservoirs, but the amount of information we obtain from geologists is also increasing. Many scientists argue to use parallel computing in order to tackle the great number of information, but this is still a subject for debate.

Appendix A

Nomenclator

In this appendix, we will give all the parameters we have used in this thesis. To the left, the symbol is given. In the middel, we give a description of the parameter. To the right, the units is given by the SI-system. Dimensionless parameters have unit 1.

Symbol	Description	Unit
A	Area	m^2
D	Coarse grid region	m^2
D^*	Coarse scale diffusion correction	1
d	Distance	m
$F(S)$	Fractional flow function	1
$f(S)$	Convensional flow function	1
$f_g(S)$	Gravity term of the fractional flow function	1
$\overline{f}(S)$	Averaged convensional flow function	1
$\widetilde{f}(S)$	Spartial varying fluctating conventional flow function	1
G^*	Coarse scale flux function	1
g	Acceleration of gravity	ms^{-2}
K	Absolute permeability	m^2
δK	Change in absolute permeability	m^2
K^*	Upscaled absolute permeability	m^2
K_e	Effective permeability	m^2
k	Relative permeability	1

Symbol	Description	Unit
K_d	Permeability in deformation bands	m^2
K_m	Permeability in the matrix	m^2
Lx	Domain length in x-direction	m
Lz	Domain length in z-direction	m
L_1	Length of a coarse grid cell in x-direction	m
L_2	Length of a coarse grid cell in y-direction	m
l_1	Length of a fine grid cell in x-direction	m
l_2	Length of a fine grid cell in y-direction	m
N	Number of deformation bands	1
N_c	Number of coarse blocks	1
N_f	Number of fine blocks	1
m^*	Coarse scale convective correction	1
$\mathbf{n}$	Outer normal vector	1
P_c	Capillary pressure	$kgm^{-1}s^{-2}$
p	Pressure	$kgm^{-1}s^{-2}$
δp	Change in pressure	$kgm^{-1}s^{-2}$
$\overline{\frac{dp}{dx}}$	Average pressure gradient	$kgm^{-1}s^{-2}$
Q	Source or sink term in mass the mass conservation law	kg
q	Flux of mass	$kgm^{-2}s^{-1}$
q_1	Flow rate in x-direction	m^3s^{-1}
q_2	Flow rate in y-direction	m^3s^{-1}
q^*	Coarse scale flow	m^3s^{-1}
r	Radius	m
S	Saturation	1
$\overline{S}$	Averaged saturation	1
$\widetilde{S}$	Spartial varying fluctating saturation	1
$\widehat{S}$	Expected saturation	1
$\overline{S}$	Averaged saturation	1
S^*	Coarse scale saturation	1
S_{BL}	Buckley-Leverett shock saturation	1
T	Transmissibility	m^2
t	Time	s
$\mathbf{u}$	Darcy velocity	ms^{-1}
$\overline{\mathbf{u}}$	Averaded Darcy velocity	ms^{-1}
$\widetilde{\mathbf{u}}$	Spartial varying fluctating Darcy velocity	ms^{-1}
$\widehat{\mathbf{u}}$	Expected velocity	ms^{-1}
$\mathbf{u}^*$	Coarse scale Darcy velocity	ms^{-1}
V	Volume	m^3
V_b	Block volume	m^3
V_p	Volume of connected pores	m^3

Symbol	Description	Unit
w	Width of the deformation bands	m
x^*	Coarse scale	1
x	Physical space coordinate	m
y	Physical space coordinate	m
z	Physical space coordinate	m
Γ	Gravity parameter	1
δ	A scalar which defines overlapping domains	1
ϵ	Scaling factor	1
η	Power averaging potens	1
θ	Angle	1
λ	Mobility	1
μ	Viscocity (assumed to be constant in this thesis)	1
ρ	Density	kgm^{-3}
σ	Surface tension	kgs^{-2}
τ	Iteration number	1

Appendix B

Coding

We will here present all codes we have used in the thesis.

B.1 Constructing Surfaces in Irap RMS

Irap RMS recieve information about faults, which are constructed in Havana, when they intersect with a surface. As we mentioned in Chapter 5, it is important that the distance between each surface is not too large such that we are able to capture the geometry of small faults. This is the reason for why we have chosen $n = 200$ in the code. In all our cases where we have constructed surfaces, we have called the top surface "Topp" and the bottom surface "Bunn". These surfaces form the upper and lower boundary of the reservoir volume. We have saved these surfaces in the file structur which is given in the algorithm, see Algorithm 1.

B.2 Constructing Faults in Havana

Havana is a program for simulating subseismic faults in petroleum reservoirs, and for integrating the effects of these faults into the reservoir description. As input we use a .dat file which must fullfill some criteria given in the user guide for the Havana software, see (2, p.208-209). Havana then constructs elliptic faults. Actually we wanted to implement deterministic faults, but this is not possible to do in Havana. This problem is reported to researchers at Norsk Regnesentral A/S, but it is uncertain whether it is possible to use deterministic data in upcoming versions. The coordinate points in the file is given on one line, in our case $z = 1000$, and the other parameters define the characterization of each fault such as length, dip, strike and reverse drag. In our geological model, we have constructed 176 faults by using Havana. As we

Algorithm 1 Script for constructing surfaces in Irap RMS

```
// This script exports the surfaces used by Havana to a sub folder named surfaces

// Declare local variables to be used
Int i,n
String horizon_name, surface_name, file_name
Surface s

// Save top surface
horizon_name = "Topp"
surface_name = "DepthSurface"
GetHorizonData(horizon_name, surface_name, s)
file_name = ".../output_rms_to_havana/surfaces/surface_top.s"
Save(s, file_name, IRAP, ASCII)

// Save n evenly spaced surfaces between top and bottom
n = 200
  for i = 1...n do
    // NOTE! The scalar is the spacing to be used between the surfaces
    s = s + 1
    file_name = ".../output_rms_to_havana/surfaces/surface_"+i+".s"
    Save(s, file_name, IRAP, ASCII)
  end for

// Save bottom surface
horizon_name = "Bunn"
surface_name = "DepthSurface"
GetHorizonData(horizon_name, surface_name, s)
file_name = ".../output_rms_to_havana/surfaces/surface_bottom.s"
Save(s, file_name, IRAP, ASCII)
```

can see in the Havana code, Algorithm 2, we include an ACTION Simulate class. This is indeed not nesseccary in our case, but we experienced that it was the only way we could include our .dat file. The ACTION Simulate class constructs faults in a stochastical fashion. Since we only wanted to implement faults given in the .dat file, we defined all the necessary stochastic variables to be so small compared to faults in the .dat file such that the code did not construct these faults. ACTION ConvertToRMS offer us the possibility to implement the faults in Irap RMS. Finally we have a class ACTION IntoPermeability which gives each fault a permeability value, in our case 1000mD.

Algorithm 2 Script for constructing faults in Havana

// This script constructs faults in Havana and is imported into Irap RMS afterwards

```
OUTPUT_LOG                      log/logfile.dat\
LEVEL_OF_INFORMATION            2 \

ACTION                          Simulate \
  INPUT_FAULTS                  skalert_data.dat \
  SIMULATION_VOLUME             output_rms_to_havana/surfaces/
                                surface_top.s
                                output_rms_to_havana/surfaces/
                                surface_bottom.s \
  NUMBER_OF_FAULTS              10 \
  DISPLACEMENT                  Range 0.005 0.015
                                FractualDimension 0.01 \
  FAULT_DISPLACEMENT_LENGTH     1 0.1 0.01 \
  FAULT_LENGTH_HEIGHT           0.5 0.01 \
  FAULT_AVERAGE_REVERSDRAG      0.1 0.01 \
  STRIKE                        Limits 0 5
                                Gaussian
                                        Expectation
                                                Constant 2.5
                                        Stdev
                                                Constant 0.01
                                \
  DISPLACEMENT                  ProbDownEast 1.0
                                ProbNormal 1.0
                                Expectation
                                        Constant 60
                                Stdev
                                        Constant 5.0
                                \
  FAULT_TRUNCATION              1 \
  NUMBER_OF_FAMILIES            13 \
  CHILDREN_PARAMETERS           0.01 0.01 0.01 \
  CHILDREN_STRIKE               0.05 \
  CHILDREN_DIP                  0.05 \
  OUTPUT_HAVANA_FAULTS          output_havana_to_rms/outhfdir \
  FAULTS_STATISTICS             output_havana_to_rms/
                                statistics.dat \
```

```
ACTION                      ConvertToRMS \
  INPUT_FAULTS              skalert_data.dat \
  OUTPUT_RMS_FAULTS         output_havana_to_rms/rms_faults \
  INPUT_SEISMIC_HORIZONS    output_rms_to_havana/surfaces/
                            surface_top.s
                            output_rms_to_havana/surfaces/surface_1.s
                            output_rms_to_havana/surfaces/surface_2.s
                            ⋮
                            output_rms_to_havana/surfaces/
                            surface_200.s
                            output_rms_to_havana/surfaces/
                            surface_bottom.s \

ACTION                      IntoPermeabilities \
  INPUT_FAULTS              output_havana_to_rms/outhfdir \
  FAULT_PERMEABILITY        1000 \
  NO_DISPLACEMENT           \
  INPUT_ECLIPSE             output_havana_to_rms/grids/
                            GridWithPerm.GRDECL \
  OUTPUT_ECLIPSE            output_havana_to_rms/grids/
                            GridWithModPerm.GRDECL \
```

B.3 Constructing the Fracture Network Model in Irap RMS

After we have constructed faults in Havana, they are imported back to Irap RMS. We will in this section present the code which constructs the fracture network model. The disadvantage of this code, is that the width of the faults depends on the grid. The code is written by Henning Nøttveit.

B.4 Flow Simulation by using the Reservoir Simulator Eclipse

We will here present the model file we are running in Eclipse. It is the same for all cases, despite for that we have to change the placement of wells since the size of the grid cells is not equal in our numerical models. We want all the flow scenarios to be as equal as possible. We do not allow any large

Algorithm 3 An IPL job in RMS constructing the fracture network model

```
Zone z = @ZONES[1]
// Declare the variables to be used
Int i,j,k
Parameter p,px,py,pz,fm
px = z.PERMX − z.PermX
py = z.PERMY − z.PermY
pz = z.PERMZ − z.PermZ
fm = z.FractureNetworkModel

p = px + py + pz

  for k = 1...z.layers − 1 do
    for i = 1...z.columns do
      for j = 1...z.rows do
        if p[i, j, k] = 0 AND p[i, j, k + 1] > 0 then
          if p[i − 1, j, k] > 0 OR p[i + 1, j, k] > 0 OR p[i, j − 1, k] > 0 OR
          p[i, j + 1, k] > 0 then
            p[i, j, k] = p[i, j, k + 1]
          end if
        end if
      end for
    end for
  end for

fm = 0

  for i = 1...z.columns do
    for j = 1...z.rows do
      for k = 1...z.layers do
        if p[i, j, k] > 0 then
          fm[i, j, k] = 1
        end if
      end for
    end for
  end for

z.FractureNetworkModel = fm
```

stepsizes because it will result in convergence problems. The code below is uncompleted when it comes to coments and describtions of each keyword, but a skilled Eclipse-user will have no problem to use the code and understand all numbers.

The model file we use in Eclipse

```
RUNSPEC
TITLE


MESSAGES
2       10*     8* /

DIMENS
1000    1       100 /

OIL

WATER

METRIC

EQLDIMS
1       100     20      1       20 /

TABDIMS
1       1       20      20      40      20 /

WELLDIMS
2       51      1       2 /

NUPCOL
10 /

START
1 'JAN' 2005 /

NSTACK
65 /
```

NOECHO

GRID
INCLUDE
EclipsePerm.GRDECL /

INIT

PROPS
ECHO

SWOF

–Sw	krw	kro	Pc
0.20	0.000	0.850	0
0.25	0.006	0.727	0
0.30	0.013	0.613	0
0.35	0.022	0.509	0
0.40	0.032	0.414	0
0.45	0.043	0.330	0
0.50	0.057	0.255	0
0.55	0.071	0.189	0
0.60	0.087	0.133	0
0.65	0.105	0.087	0
0.70	0.124	0.051	0
0.75	0.144	0.024	0
0.80	0.167	0.007	0
0.85	0.190	0.000	0
0.90	0.215	0.000	0
0.95	0.400	0.000	0
1.00	1.000	0.000	0 /

PVTW

302.2	1.024	$4.64 * 10^{-5}$	0.42 /

ROCK
1.0 0.000056 /

DENSITY

–Oil	Water	Gas
241.5	241.5	0.330 /

```
PVDO
–P              Bo              viscO
17              1.2907          0.8541
47              1.2877          0.8811
77              1.2847          0.9081
107             1.2817          0.9351
137             1.2787          0.9621
167             1.2757          0.9891
197             1.2727          1.0161
227             1.2600          1.0420
253.4           1.2555          1.0720
281.6           1.2507          1.0960
311.1           1.2463          1.1180
343.8           1.24173         1.1510
373.3           1.2377          1.174
395.5           1.2356          1.200
500.0           1.2257          1.322 /

SOLUTIONS
EQUIL
900     320.0   1110    0       1100    0       1       0       0 /

RPTSOL
FIP=1           RESTART=2 /

SUMMARY
ELAPSED
FOPR
FOPT
FWPR
FWPT
FWIR
FWCT
FPR
RPR
/
FGOR
FOIP
FGPR
FOE
```

```
FOIP
ROIP
/
WWCT
/
WBHP
/

SCHEDULE
RPTRST
BASIC=5       NORST=1       FREQ=2 /

WELSPECS
'WP1'  'G'    12     1      1*     'OIL' /
'WI1'  'G'    987    1      1*     'WATER' /

COMPDAT
'WP1'  0      0      1      50     'OPEN' 0      -1     0.3
-1     0      0      'Z' /
'WI1'  0      0      50     100    'OPEN' 0      -1     0.3
-1     0      0      'Z' /

WCONPROD
'WP1'  'OPEN'        'LRAT' 3*     30     1*     17     3*0 /

WCONINJE
'WI1'  'WATER'       'OPEN'        'RATE' 35     1*
500    1* /

WECON
'WP1'  2*     1      2*     WELL   YES /

GECON
'FIELD'2*     1      2*     WELL   YES /

TUNING
0.1    2 /
/
12     1      100    1      20 /

DATES
```

```
1 'APR' 2005 /
1 'JUL' 2005 /
1 'OCT' 2005 /
1 'JAN' 2006 /
/

WCONPROD
'WP1'   'OPEN'          'LRAT' 3*       15      1*      17      3*0 /

WCONINJE
'WI1'   'WATER'         'OPEN'          'RATE' 18       1*
500     1* /

DATES
1 'APR' 2006 /
1 'JUL' 2006 /
.
.
.
1 'JAN' 2017 /
/

END
```

Appendix C

Effect of Gravity in Eclipse

In this appendix, we will demonstrate the effect of setting the density equal for both phases (oil and water). Setting the density equal is done in order to neglect the effect of gravity in Eclipse. We have constructed a model where we have transformed the x- and z-values such that, despite of where we are on the x-coordinate, the water front will have the same effect of gravity. This model is compared with the fine scale simulation we have used in this thesis. Both scenarios simulated the fluid flow in 12 years. Figure C.1 and Figure C.2 show that by setting the density to be equal for both phases, we have almost the same fluid flow as when we rotate the coordinate system. Figure C.3 illustrates a simulation run where we have used physically correct values for the density. Although we can see that the water front in C.1 has moved longer at 1. January 2012 and 1. January 2017 compared with the same dates in Figure C.2, we can conclude with that the effect of gravity is considerable reduced by comparing Figure C.2 with Figure C.3.

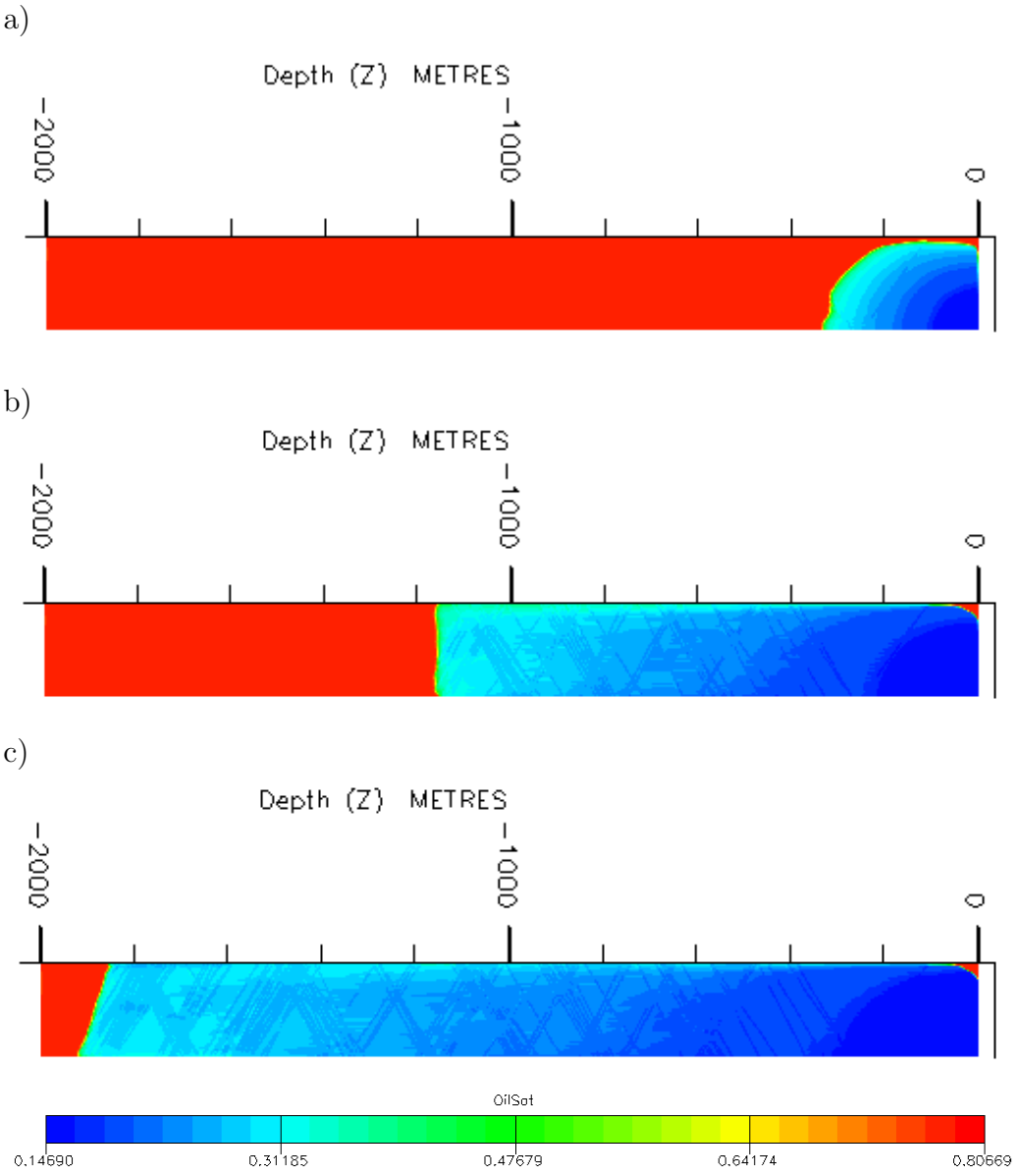

Figure C.1: Simulation results for a rotated system after a) 1. January 2006 b) 1. January 2012 c) 1. January 2017. The x-axis gives the distance while the z-axis indicates the depth, both measured in meters.

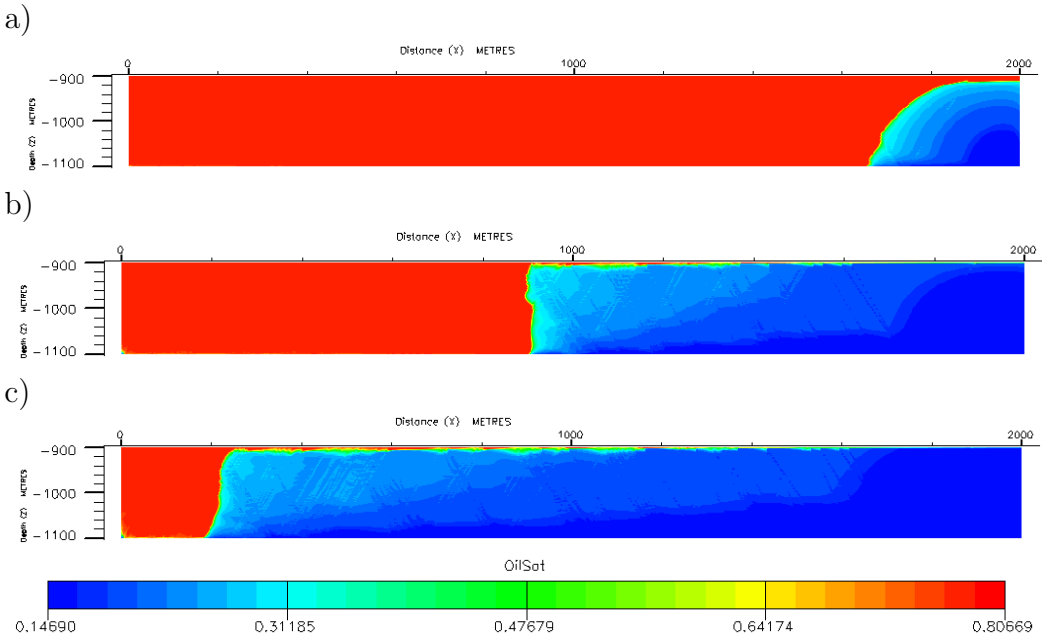

Figure C.2: Fine scale simulation results after a) 1. January 2006 b) 1. January 2012 c) 1. January 2017. The x-axis gives the distance while the z-axis indicates the depth, both measured in meters.

a)

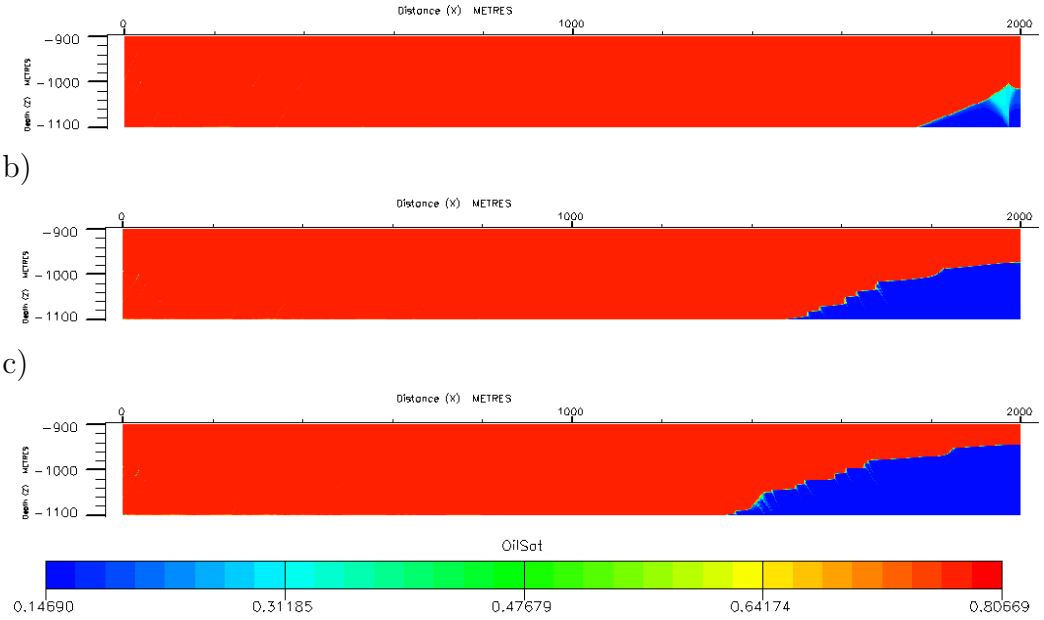

Figure C.3: Fine scale simulation results with no changes in the density after a) 1. January 2006 b) 1. January 2012 c) 1. January 2017. The x-axis gives the distance while the z-axis indicates the depth, both measured in meters.

References

[1] J. E. Aarnes. *On Numerical Methods for Multifield Problems and Fast Reservoir Performance Prediction*. PhD thesis, University of Bergen, Norway, 2002.

[2] SAND: Statistical analysis of natural resources. Havana la aurora user's manual version 5.5. Technical report, Norwegian Computing Center, 2007.

[3] T. M. Apostol. *Calculus, Volume* 2. John Wiley & Sons, 1969.

[4] J. W. Barker and S. Thibeau. A critical review of the use of pseudo-relative permeabilities for upscaling. *SPE Res. Eng.*, 1997.

[5] S. S. Berg and E. Øian. Hierarchical approach for simulating fluid flow in normal fault zones. *Petroleum Geoscience*, 2007.

[6] Ø. Bøe. Analysis of an upscaling method based on conservation of dissipation. *Transport in Porous Media*, 1994.

[7] J. S. Caine, J. P. Evans, and C. B. Forster. Fault zone architecture and permeability structure. *Geology*, 1996.

[8] Y. Chen and L.J. Durlofsky. Adaptive local-global upscaling for general flow scenarios in heterougeneous formations. *Transport in Porous Media*, 2006.

[9] Y. Chen, L.J. Durlofsky, M. Gerritsen, and X.H. Wen. A coupled local-global upscaling approach for simulating flow in highly heterogeneous formations. *Advances in Water Resources*, 2003.

[10] M. A. Christie. Flow in porous media - scale up of multiphase flow. *Colloid and Interface Science*, 2001.

[11] R. E. Collins. *Flow of Fluids through Porous Materials*. Tulsa, PennWell-Books, 1961.

[12] H. Darcy. *Les FontainsPubliques de la Ville de Dijon*. Victor Dalmont, Paris, 1856.

[13] G. H. Davies and S. J. Reynolds. *Structural Geology of Rocks and Regions*. John Wiley & Sons, 1996.

[14] L.J. Durlofsky. Numerical calculation of equivalent grid block permeability tensors for heterogenous porous media. *Water Resources Research*, 1991.

[15] L.J. Durlofsky. Use of higher moments of the description of upscaled, process independent relative permeabilities. *SPE Journal*, 2, 1997.

[16] L.J. Durlofsky. Coarse scale models of two phase flow in heterogeneous reservoirs: volume averaged equations and their relastionship to existing upscaling techniques. *Computational Geosciences*, 1998.

[17] L.J. Durlofsky. Upscaling and gridding of fine scale geological models for flow simulation. *Presented at the* 8^{th} *International Forum on Reservoir Simulation Iles Borromees, Stresa, Italy*, 2005.

[18] L.J. Durlofsky and J.F. Brady. Analysis of the Brinkman equation as a model for flow in porous media. *Phys. Fluids*, 1987.

[19] Y. Efendiev and L. J. Durlofsky. Numerical modeling of subgrid heterogeneity in two phase flow simulations. *Water Resources Research*, 2002.

[20] Y. Efendiev and L. J. Durlofsky. A generalized convection-diffusion model for subgrid transport in porous media. *Multiscale Modeling Simulation*, 2003.

[21] C. L. Farmer. Upscaling: a review. *International journal for numerical methods in fluids*, 2002.

[22] H. Fossen and A. Bale. Deformation bands and their influence on fluid flow. *AAPG Bulletin*, 2007.

[23] H. Fossen, R. A. Schultz, Z. K. Shipton, and K. Mair. Deformation bands in a sandstone: a review. *Journal of the Geological Society*, 2007.

[24] R. A. Freeze. A stochastic-conseptual analysis of one-dimensional groundwater flow in nonuniform homogenuous media. *Advanced in Water Resources*, 1975.

[25] K. J. Hersvik and M. S. Espedal. Adaptive hierarchical upscaling of flow in heterougeneous reservoirs based on an posteriori error estimate. *Computational Geosciences*, 1998.

[26] L. Holden and B. F. Nielsen. Global upscaling of permeability in heterogenous reservoirs: The output least squares (ols) method. *Transport in Porous Media*, 2000.

[27] R. Holm, Roland Kaufmann, Bjørn-Ove Heimsund, Erlend Øian, and Magne S. Espedal. Meshing of domains with complex internal geometries. *Numerical Linear Algebra with Applications*, 2006.

[28] M. J. King and M. Mansfield. Flow simulation of geologic models. *SPE Reservoir Evaluation and Engineering*, 1999.

[29] P. Langlo and M.S. Espedal. Macrodispersion for two-phase, immiscible flow in porous media. *Advanced in Water Resources*, 1994.

[30] S. H. Lee, M. F. Lough, and C. L Jensen. Hierarchical modeling of flow in naturally fractured formations with multiple length scales. *Water Resources Research*, 2001.

[31] S. Marshak. *Earth: Portrait of a Planet*. W. W. Norton & Company, 2001.

[32] Ø. Pettersen. *Basics of Reservoir Simulation with the Eclipse Reservoir Simulator - Lecture Notes*. University of Bergen, Norway, 2006.

[33] Y. Rubin and J.J. Gómez-Hernández. A stochastic approach to the problem of upscaling of conductivity in disorder media: Theory and unconditional numerical simulations. *Water Resour. Res.*, 1990.

[34] M. Sahimi. *Flow and Transport in Porous Media and Fractured Rock: From Classical Methods to Modern Approaches*. Wiley-VCH Verlag GmbH, 1995.

[35] R. C. Selly. *Elements of Petroleum Geology*. Academic Press, 1998.

[36] K. S. Sorbie and M. I. J. van Dijke. Fundamentals of three-phase flow in porous media of heterogeneous wettability. September 2004.

[37] E. A. Sudicky. A natural gradient experiment on solute transport in a sand aquifer: Spartial variability of hydraulic conductivety and its role in the dipersion process. *Advanced in Water Resources*, 1986.

[38] C. B. Tjølsen and E. Damsleth. A model for the simultaneous generation of core-controlled stochastic absolute and relative permeability fields. *Proc.* 66^{th} *Ann. Technical Conf. of SPE, Dallas*, 1991.

[39] X. H. Wen, L. J. Durlofsky, and M. G. Edwards. Upscaling of channel systems in two dimensions using flow-based grids. *Transport in Porous Media*, 2003.

[40] X. H. Wen, L. J. Durlofsky, and M. G. Edwards. Use of border regions for improved permeability upscaling. *Mathematical Geology*, 2003.

[41] R. J. M. De Wiest. *Flow through Porous Media*. Academic Press, 1969.

[42] X. H. Wu, Y. Efendiev, and T. Y Hou. Analysis of upscaling absolute permeability. *Discrete and Continuous Dynamical Systems*, 2002.